Electronic Supplementary Material (ESI) for Journal of Materials Chemistry C.
This journal is © The Royal Society of Chemistry 2024

Structural, Dielectric, and Conduction Behaviour of A-site deficient $Sr_xNa_{1-2x}NbO_3$ Ceramics

Thomas E. Hooper[1] and Derek C. Sinclair

Department of Materials Science and Engineering, Sir Robert Hadfield Building, University of Sheffield, Mappin Street, Sheffield S1 3JD, UK

Supplementary Information

Contents

List of Figures..... **2**

List of Tables..... **4**

SI Section S1: Analysis of reagents..... 5

SI Section S2: Analysis of calcined powders..... 7

SI Section S3: X-ray diffraction and Rietveld Refinements..... 10

SI Section S4: Microstructural Analysis..... 14

SI Section S5: Dielectric Spectroscopy..... 29

SI Section S6: Polarisation vs Electric Field analysis..... 35

SI Section S7: Impedance Spectroscopy and Arrhenius plots..... 36

[1] Corresponding author: thomas.elliot.hooper@gmail.com

List of Figures

Figure S1: Secondary electron images of reagents (a) $SrCO_3$, (b) Na_2CO_3, and (c) Nb_2O_5 after dehydration.

Figure S2: Stacked X-ray diffraction patterns from 10-100° 2θ (Cu-Kα source) of (a) $SrCO_3$ (fully indexed to orthorhombic *Pnma*), (b) Na_2CO_3 (fully indexed to orthorhombic *Pca*2_1), and (c) Nb_2O_5 (fully indexed to orthorhombic *C*2/*c*) reagents after dehydration.

Figure S3: Particle size distributions of powders used for pressing for (a) $NaNbO_3$ (x = 0.00), (b) $Sr_{0.05}Na_{0.90}NbO_3$ (x = 0.05), (c) $Sr_{0.10}Na_{0.80}NbO_3$ (x = 0.10), (d) $Sr_{0.15}Na_{0.70}NbO_3$ (x = 0.15), (e) $Sr_{0.20}Na_{0.6}NbO_3$ (x = 0.20), and (f) $Sr_{0.25}Na_{0.50}NbO_3$ (x = 0.25). 500 particles across 3 secondary electron micrographs were measured.

Figure S4: Average d_{10}, d_{50}, and d_{90} against composition for powders used for pressing. Dotted and dashed lines represent ± 1 and ± 2 standard deviations (σ), respectively.

Figure S5: XRD patterns from 10-100° 2θ and step size 0.02° for calcined powders after first and second calcination for all compositions.

Figure S6: Rietveld refinements for (a) $NaNbO_3$, (b) $Sr_{0.05}Na_{0.90}NbO_3$, (c) $Sr_{0.10}Na_{0.80}NbO_3$, (d) $Sr_{0.15}Na_{0.70}NbO_3$, (e) $Sr_{0.20}Na_{0.60}NbO_3$, and (f) $Sr_{0.25}Na_{0.50}NbO_3$

Figure S7: Pseudo-monoclinic tilt angle ($2\tan^{-1}(c_O/b_O)$, where c_O and b_O represent the orthorhombic lattice parameters) against composition.

Figure S8: Geometric density, theoretical density calculated using lattice parameters from XRD refinements, and relative density against composition. Error bars correspond to standard error from the measurements of 5 samples.

Figure S9: Secondary electron micrographs of polished and thermally etched samples for compositions (a) $NaNbO_3$, (b) $Sr_{0.05}Na_{0.90}NbO_3$, (c) $Sr_{0.10}Na_{0.80}NbO_3$, (d) $Sr_{0.15}Na_{0.70}NbO_3$, (e) $Sr_{0.20}Na_{0.60}NbO_3$, and (f) $Sr_{0.25}Na_{0.50}NbO_3$. Particle size determined by measuring 200 individual particles across 3 secondary electron micrographs using ImageJ software.

Figure S10: Backscatter electron micrographs and corresponding EDX maps of polished and thermally etched samples of (a) $NaNbO_3$, (b) $Sr_{0.05}Na_{0.90}NbO_3$, (c) $Sr_{0.10}Na_{0.80}NbO_3$, (d) $Sr_{0.15}Na_{0.70}NbO_3$, (e) $Sr_{0.20}Na_{0.60}NbO_3$, and (f) $Sr_{0.25}Na_{0.50}NbO_3$. Bright regions in (c) and (d) can be identified as $NaNb_3O_8$ and in (f) as tetragonal tungsten bronze $Sr_2NaNb_5O_{15}$

Figure S11: Backscattered electron micrograph of polished and thermally etched $Sr_{0.10}Na_{0.80}NbO_3$ bulk ceramic, annotated with point spectra positions.

Figure S12: Backscattered electron micrograph of polished and thermally etched $Sr_{0.15}Na_{0.70}NbO_3$ bulk ceramic, annotated with point spectra positions.

Figure S13: Point spectra across a grain in polished and thermally etched $Sr_{0.20}Na_{0.60}NbO_3$ and corresponding atomic percentage to demonstrate core-shell microstructure.

Figure S14: Backscattered electron micrograph of polished and thermally etched $Sr_{0.25}Na_{0.50}NbO_3$ bulk ceramic, annotated with point spectra positions.

Figure S15: Sr^{2+} and Na^{+} occupancies extracted from Rietveld refinements (solid data points) and average at% calculated from EDX mapping (hollow data points) against composition. Dashed lines correspond to nominal $Sr_xNa_{1-2x}NbO_3$

Figure S16: (a) Real component of permittivity (ε') and (b) tan δ at fixed frequencies against temperature for $NaNbO_3$ (x = 0.00)

Figure S17: (a) Real component of permittivity (ε') and (b) tan δ at fixed frequencies against temperature for $Sr_{0.05}Na_{0.90}NbO_3$ (x = 0.05). Sub-zero tan δ are due to electrical noise (inductance) from electrical testing equipment.

Figure S18: (a) Real component of permittivity (ε') and (b) tan δ at fixed frequencies against temperature for $Sr_{0.10}Na_{0.80}NbO_3$ (x = 0.10)

Figure S19: (a) Real component of permittivity (ε') and (b) tan δ at fixed frequencies against temperature for $Sr_{0.15}Na_{0.70}NbO_3$ (x = 0.15)

Figure S20: (a) Real component of permittivity (ε') and (b) tan δ at fixed frequencies against temperature for $Sr_{0.20}Na_{0.60}NbO_3$ (x = 0.20)

Figure S21: (a) Real component of permittivity (ε') and (b) tan δ at fixed frequencies against temperature for $Sr_{0.25}Na_{0.50}NbO_3$ (x = 0.25)

Figure S22: Arrhenius plots of conductivity calculated using M'' peak height at the relaxation frequency for (a) $NaNbO_3$, (b) $Sr_{0.05}Na_{0.90}NbO_3$, (c) $Sr_{0.10}Na_{0.80}NbO_3$, (d) $Sr_{0.15}Na_{0.70}NbO_3$, (e) $Sr_{0.20}Na_{0.60}NbO_3$, and (f) $Sr_{0.25}Na_{0.50}NbO_3$.

Figure S23: High temperature and low temperature activation energies extrapolated from Arrhenius plots of conductivity against composition.

List of Tables

Table S1: Spectrum number according to Figure S11, and corresponding atomic percentage of ions. Highlighted cells correspond to regions of bright contrast.

Table S2: Spectrum number according to Figure S12, and corresponding atomic percentage of ions. Highlighted cells correspond to regions of bright contrast.

Table S3: Spectrum number according to Figure S14, and corresponding atomic percentage of ions. Highlighted cells correspond to regions of bright contrast.

Table S4: Maximum polarisation (P_{lax}), remnant polarisation (P_R), coercive filed (E_C), recoverable energy density (W_{rec}), energy loss density (W_{loss}), thickness (S) over electrode radius (r), and efficiency ($W_{rec}/W_{rec}+W_{loss}$) for $Sr_xNa_{1-2x}NbO_3$ (x = 0.00, 0.05, 0.10, 0.15, 0.20, 0.25) at 40 $kV.cm^{-1}$

SI Section S1: Analysis of Reagents

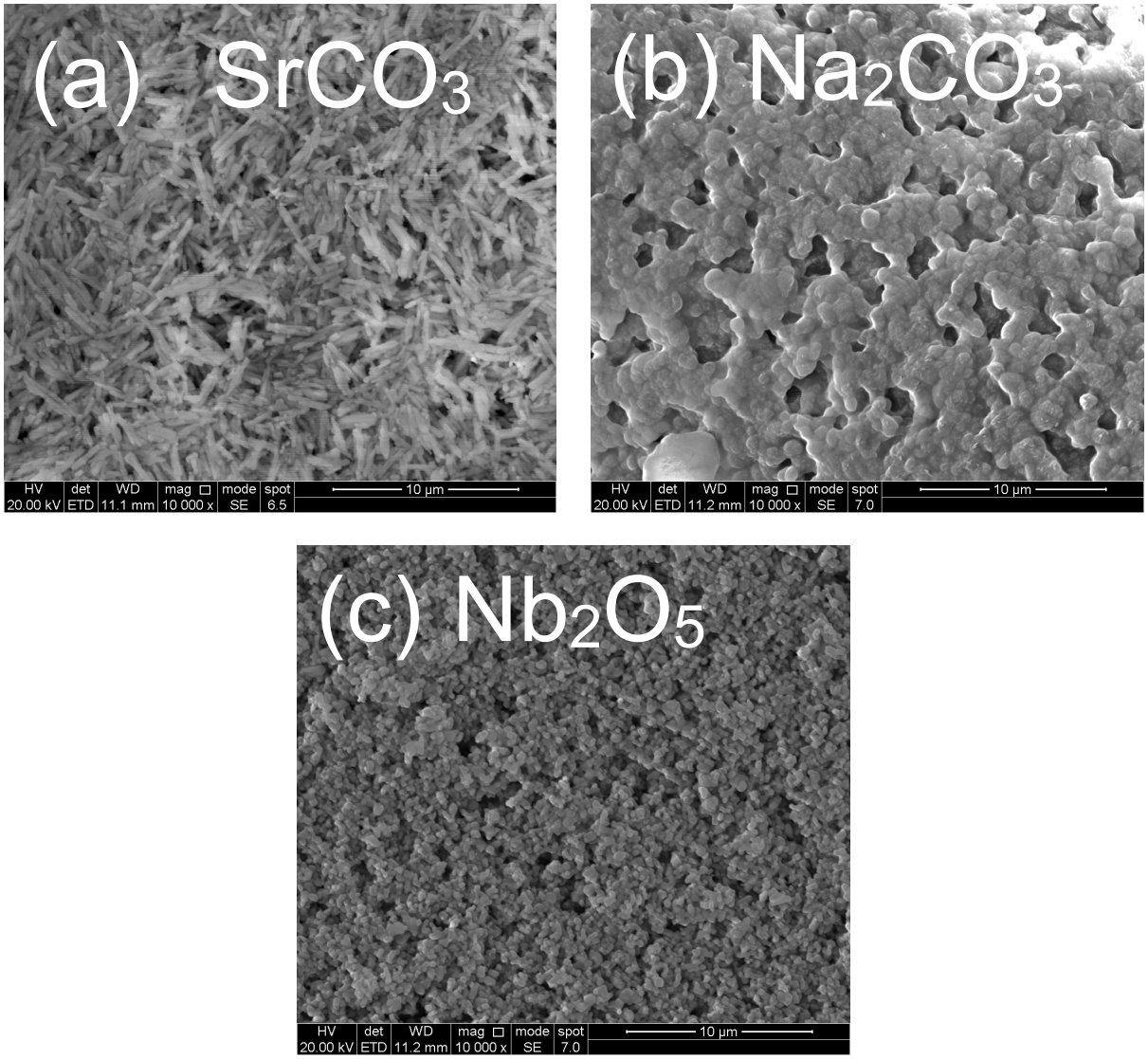

Figure S1: Secondary electron images of reagents (a) $SrCO_3$, (b) Na_2CO_3, and (c) Nb_2O_5 after dehydration.

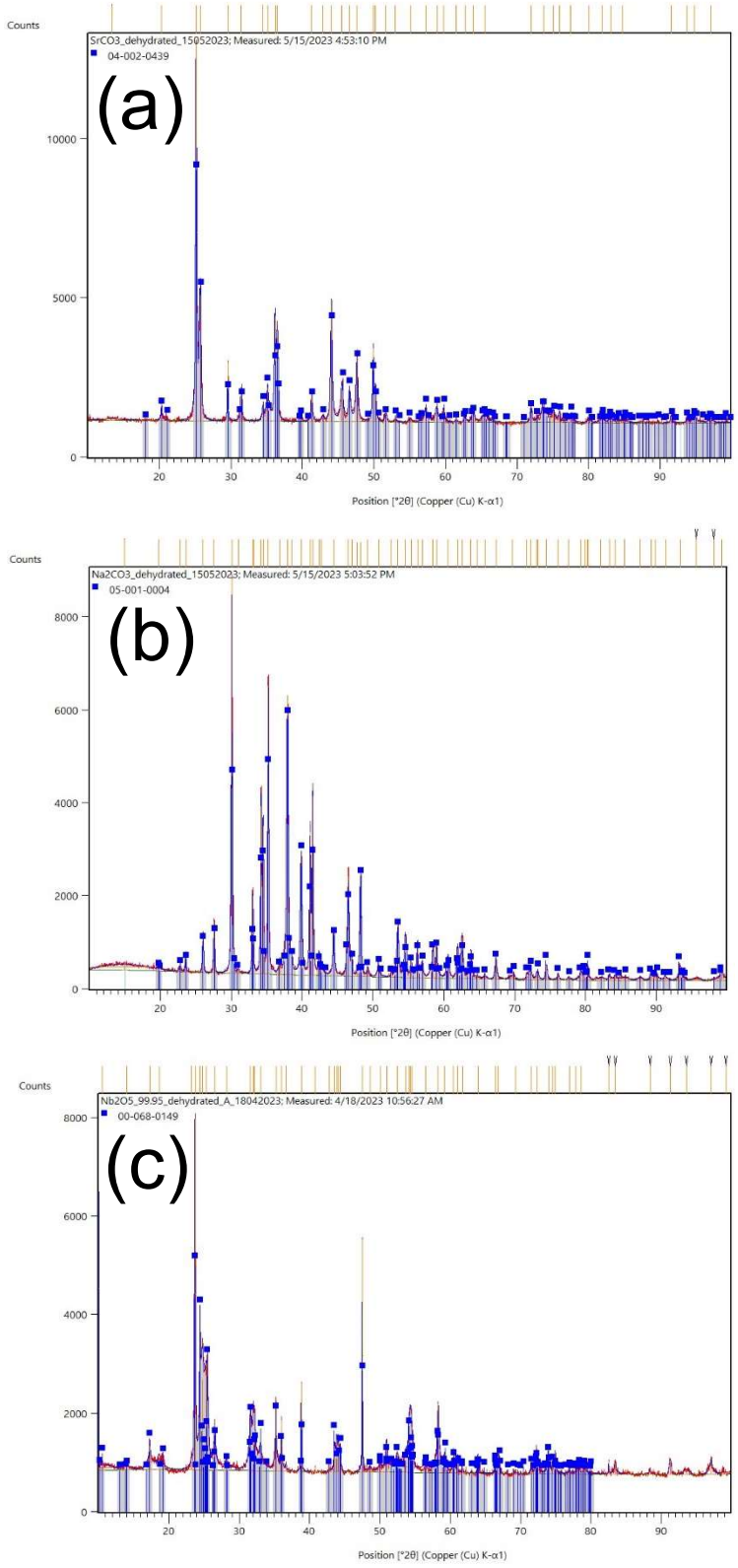

Figure S2: Stacked X-ray diffraction patterns from 10-100° 2θ (Cu-Kα source) of (a) $SrCO_3$ (fully indexed to orthorhombic *Pnma*), (b) Na_2CO_3 (fully indexed to orthorhombic *Pca*2_1), and (c) Nb_2O_5 (fully indexed to orthorhombic *C*2/*c*) reagents after dehydration.

SI Section S2: Analysis of calcined powders

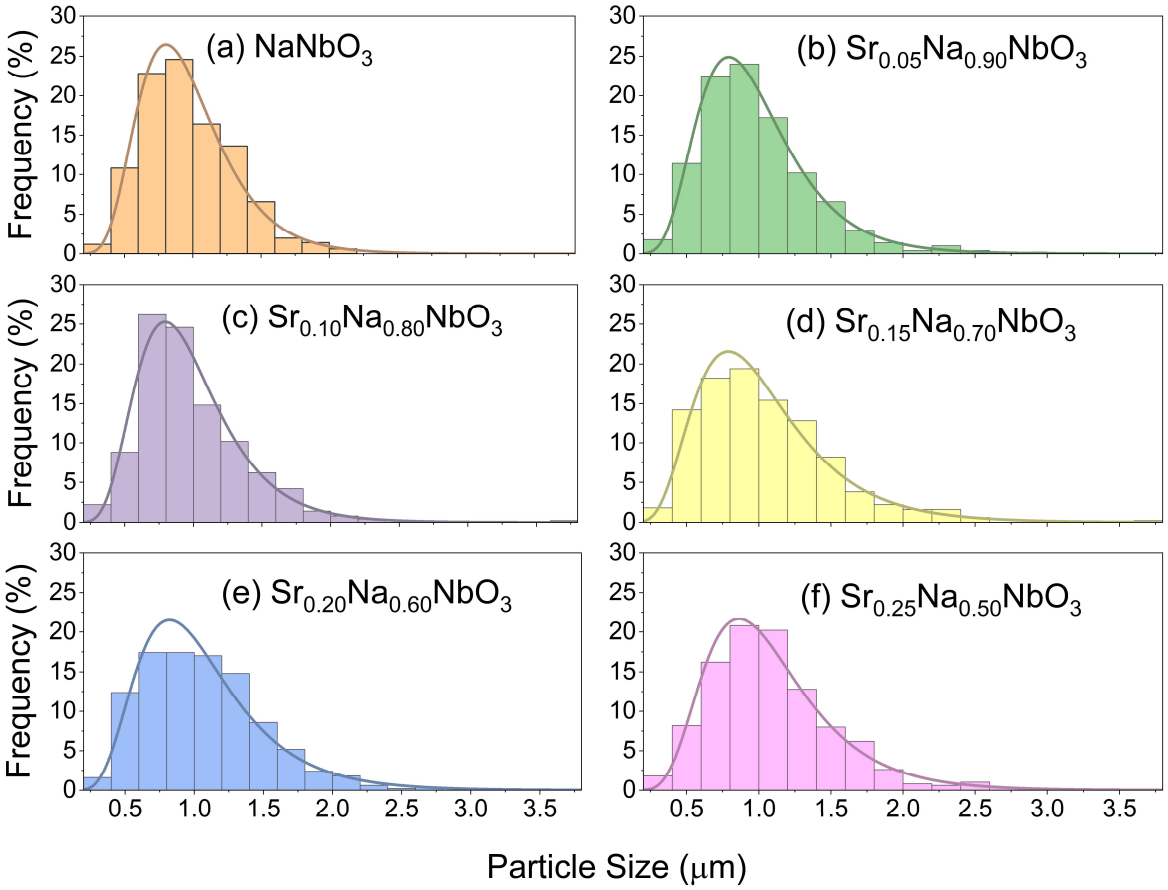

Figure S3: Particle size distributions of powders used for pressing for (a) $NaNbO_3$ (x = 0.00), (b) $Sr_{0.05}Na_{0.90}NbO_3$ (x = 0.05), (c) $Sr_{0.10}Na_{0.80}NbO_3$ (x = 0.10), (d) $Sr_{0.15}Na_{0.70}NbO_3$ (x = 0.15), (e) $Sr_{0.20}Na_{0.6}NbO_3$ (x = 0.20), and (f) $Sr_{0.25}Na_{0.50}NbO_3$ (x = 0.25). 500 particles across 3 secondary electron micrographs were measured.

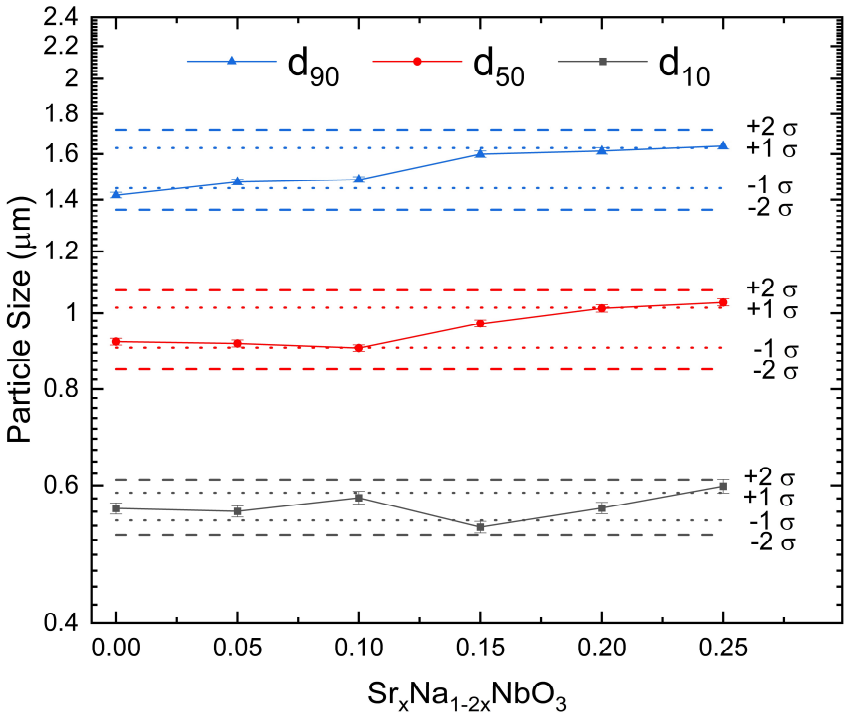

Figure S4: Average d_{10}, d_{50}, and d_{90} against composition for powders used for pressing. Dotted and dashed lines represent ± 1 and ± 2 standard deviations (σ), respectively.

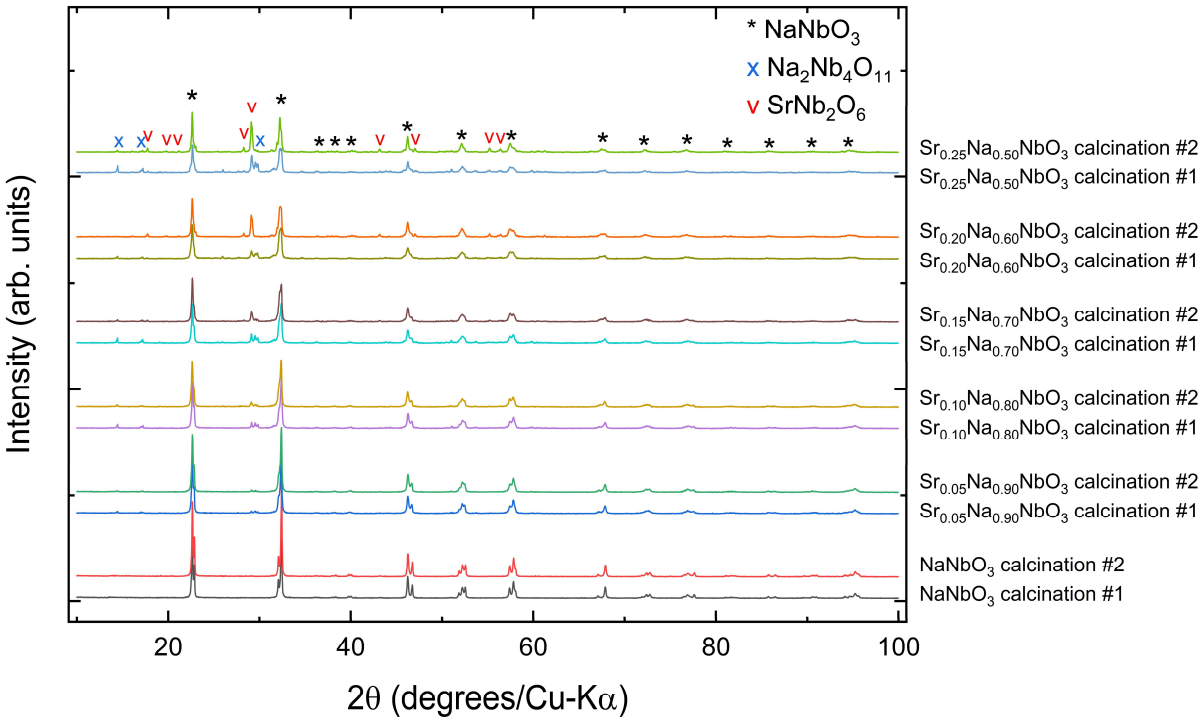

Figure S5: XRD patterns from 10-100° 2θ and step size 0.02° for calcined powders after first and second calcination for all compositions.

SI Section S3: X-ray diffraction and Rietveld Refinements

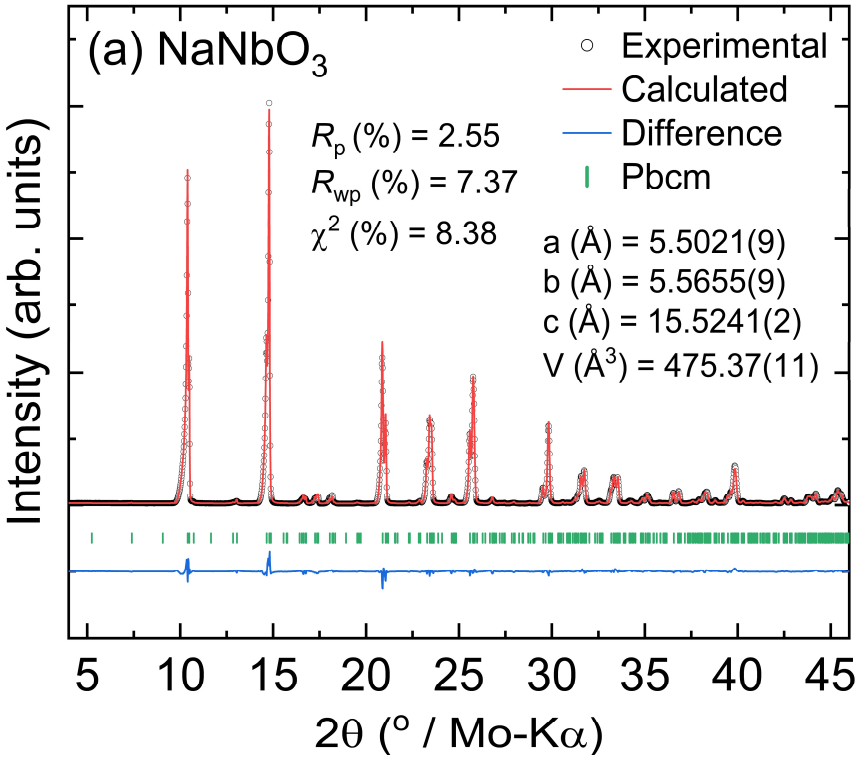

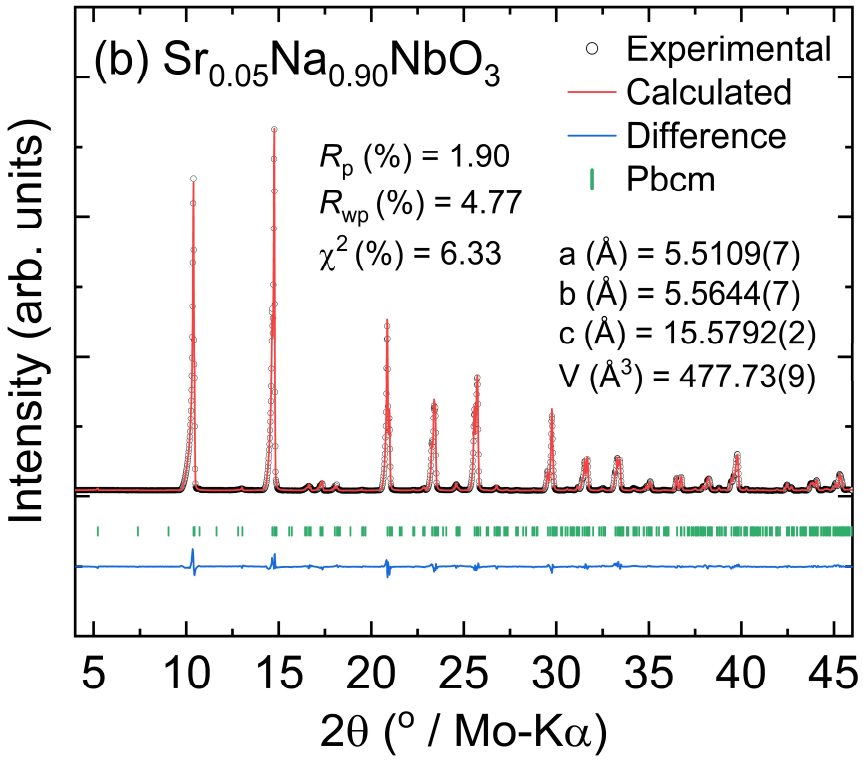

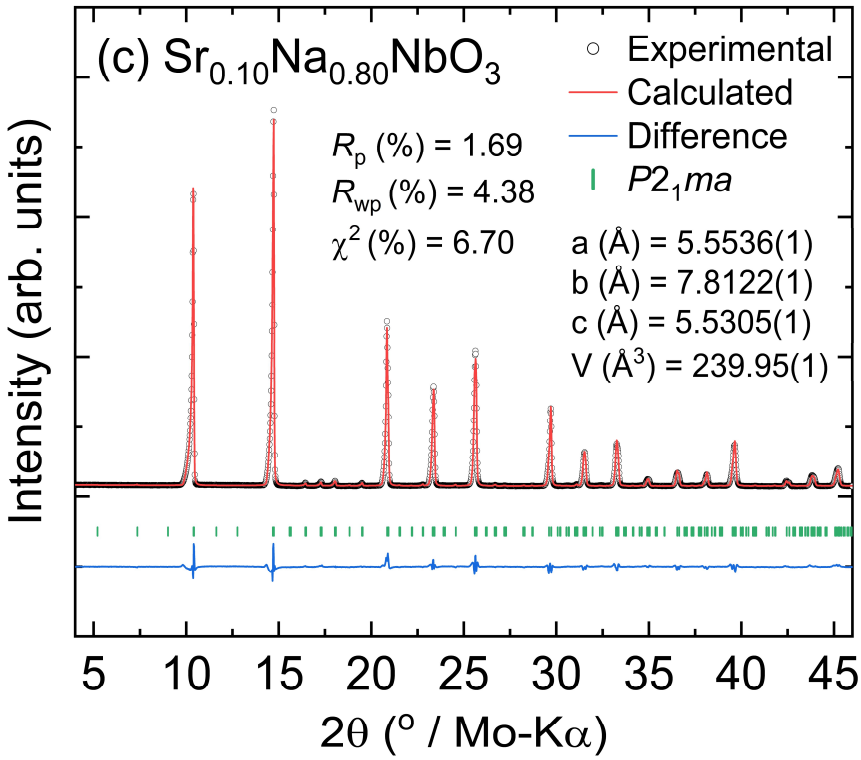
(c) Sr0.10Na0.80NbO3
Experimental
Calculated
Difference
P21ma
Rp (%) = 1.69
Rwp (%) = 4.38
χ2 (%) = 6.70
a (Å) = 5.5536(1)
b (Å) = 7.8122(1)
c (Å) = 5.5305(1)
V (Å3) = 239.95(1)
Intensity (arb. units)
5 10 15 20 25 30 35 40 45
2θ (° / Mo-Kα)

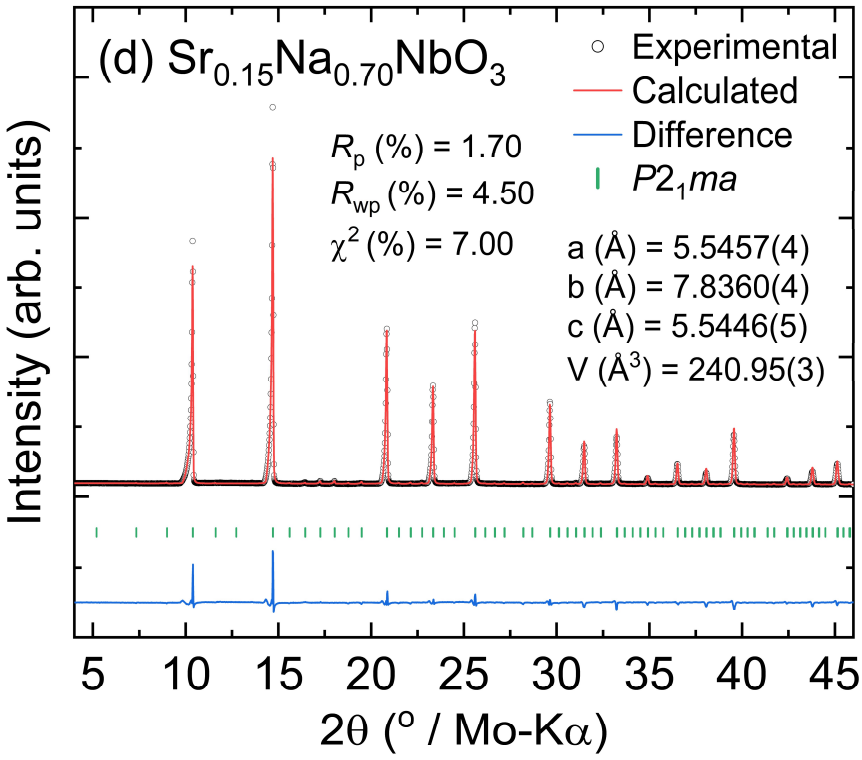
(d) Sr0.15Na0.70NbO3
Experimental
Calculated
Difference
P21ma
Rp (%) = 1.70
Rwp (%) = 4.50
χ2 (%) = 7.00
a (Å) = 5.5457(4)
b (Å) = 7.8360(4)
c (Å) = 5.5446(5)
V (Å3) = 240.95(3)
Intensity (arb. units)
5 10 15 20 25 30 35 40 45
2θ (° / Mo-Kα)

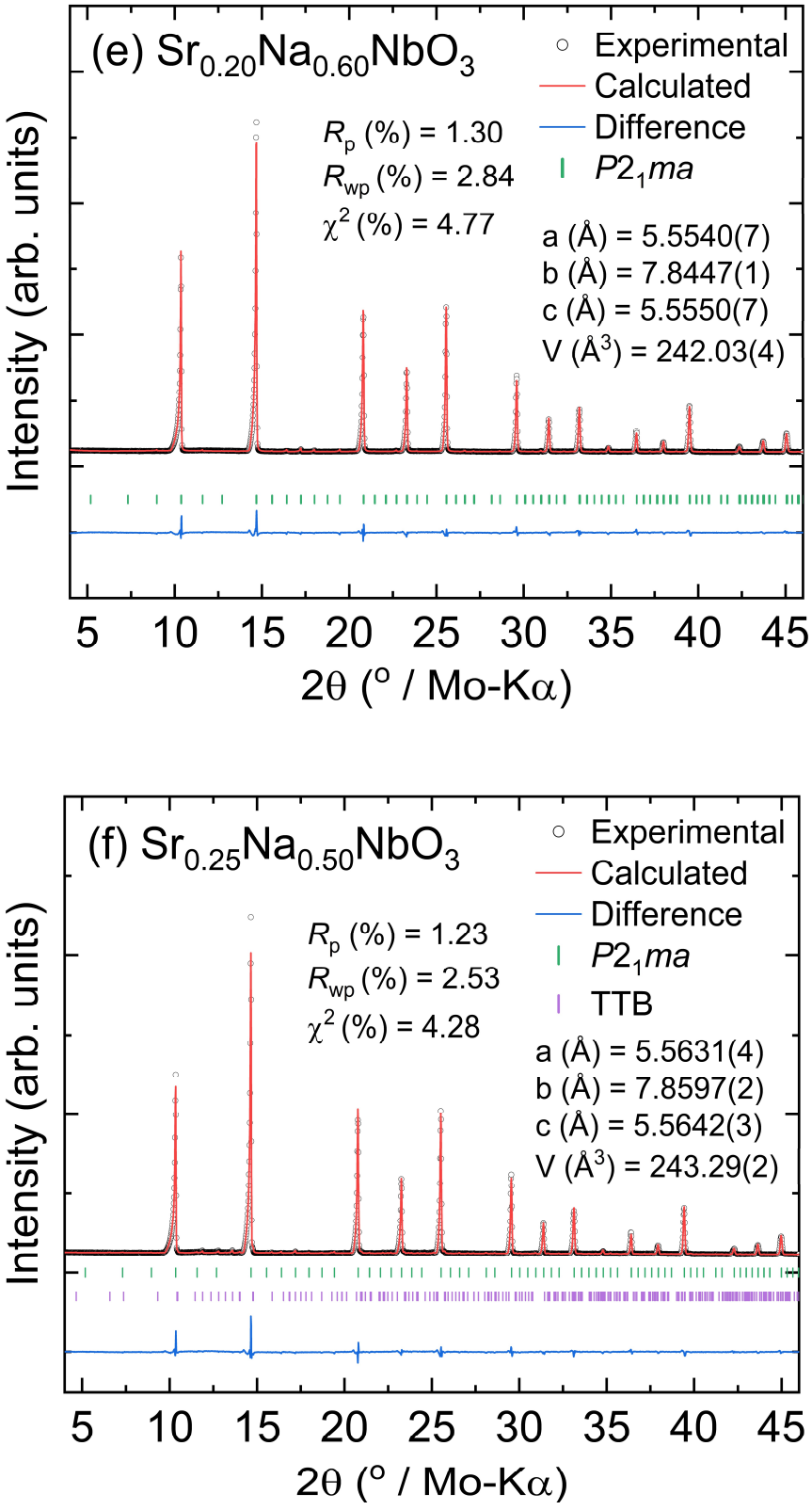

Figure S6: Rietveld refinements for (a) $NaNbO_3$, (b) $Sr_{0.05}Na_{0.90}NbO_3$, (c) $Sr_{0.10}Na_{0.80}NbO_3$, (d) $Sr_{0.15}Na_{0.70}NbO_3$, (e) $Sr_{0.20}Na_{0.60}NbO_3$, and (f) $Sr_{0.25}Na_{0.50}NbO_3$

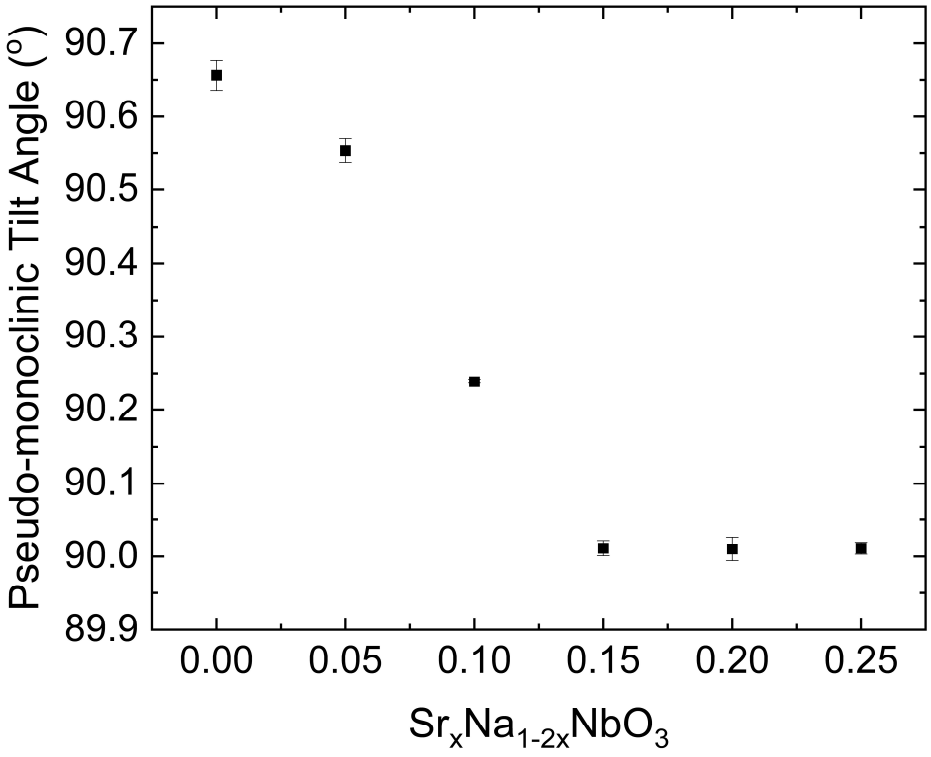

Figure S7: Pseudo-monoclinic tilt angle ($2\tan^{-1}(c_O/b_O)$, where c_O and b_O represent the orthorhombic lattice parameters) against composition.

SI Section S4: Microstructural Analysis

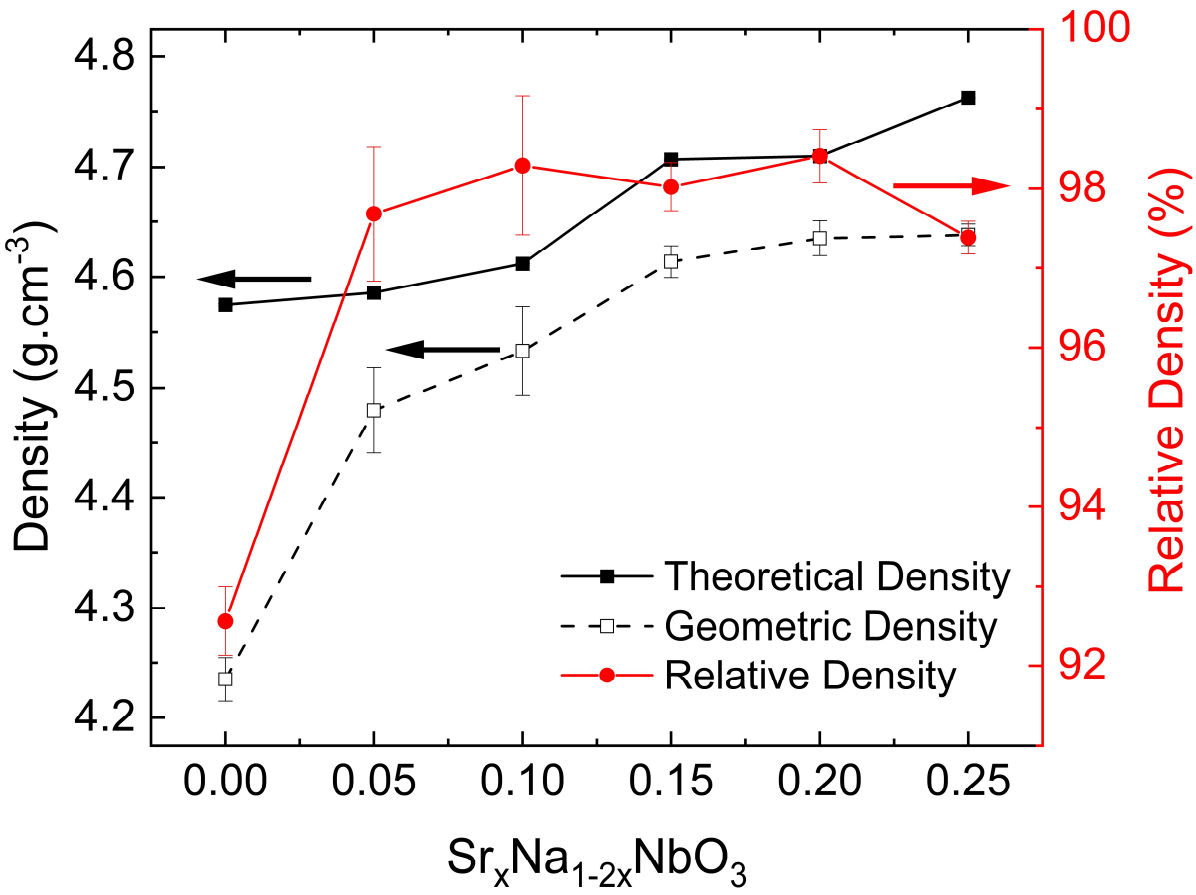

Figure S8: Geometric density, theoretical density calculated using lattice parameters from XRD refinements, and relative density against composition. Error bars correspond to standard error from the measurements of 5 samples.

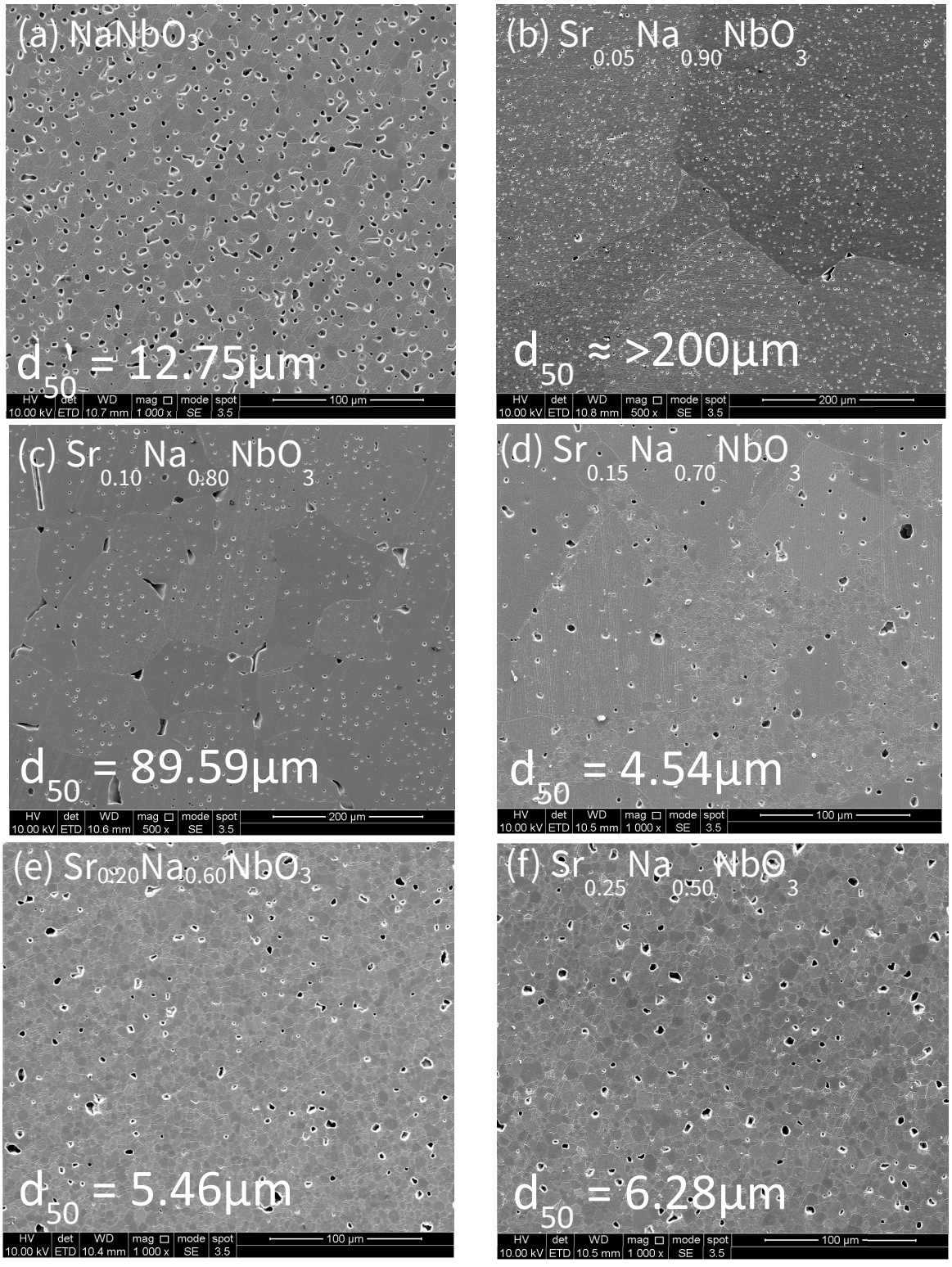

Figure S9: Secondary electron micrographs of polished and thermally etched samples for compositions (a) $NaNbO_3$, (b) $Sr_{0.05}Na_{0.90}NbO_3$, (c) $Sr_{0.10}Na_{0.80}NbO_3$, (d) $Sr_{0.15}Na_{0.70}NbO_3$, (e) $Sr_{0.20}Na_{0.60}NbO_3$, and (f) $Sr_{0.25}Na_{0.50}NbO_3$. Particle size determined by measuring 200 individual particles across 3 secondary electron micrographs using ImageJ software.

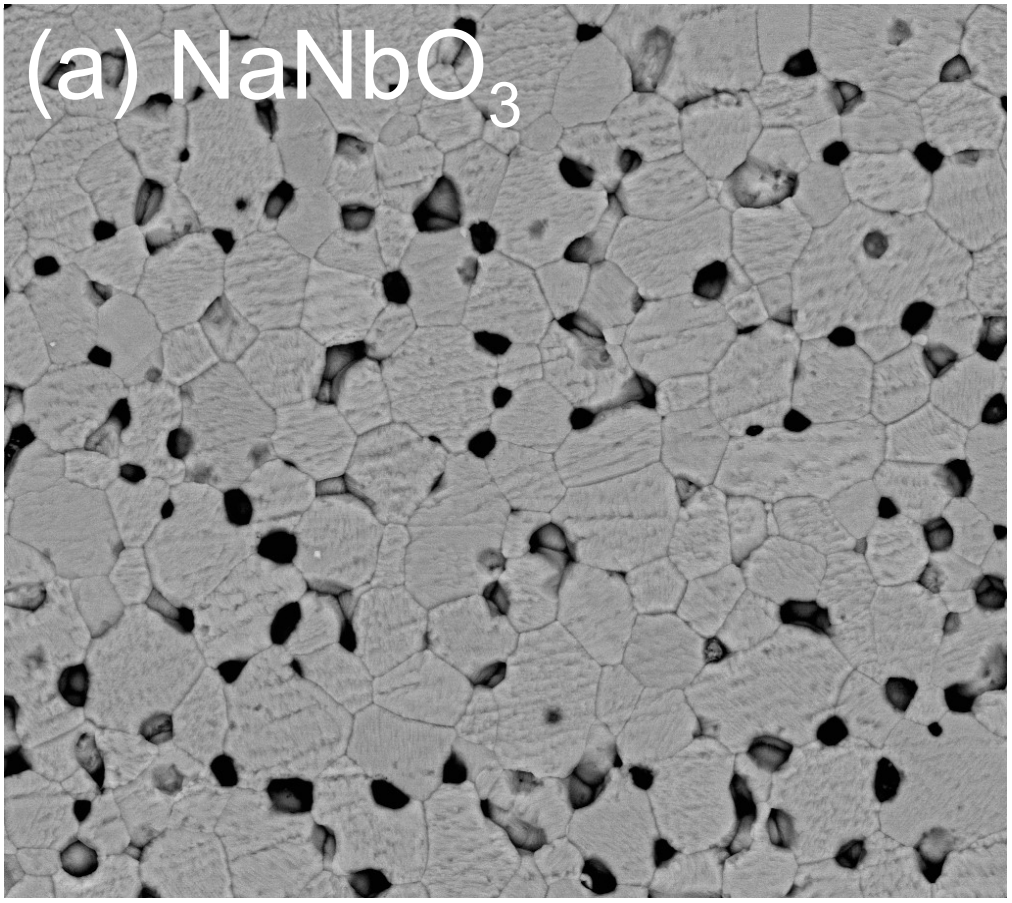
(a) NaNbO3
25μm

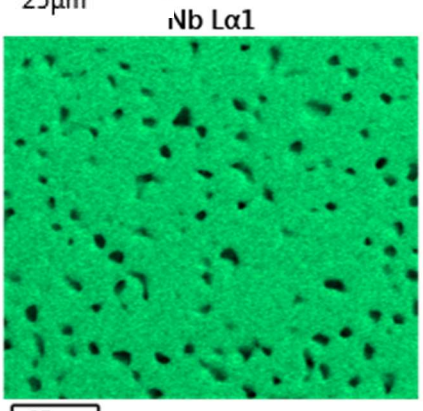
Nb Lα1
25μm

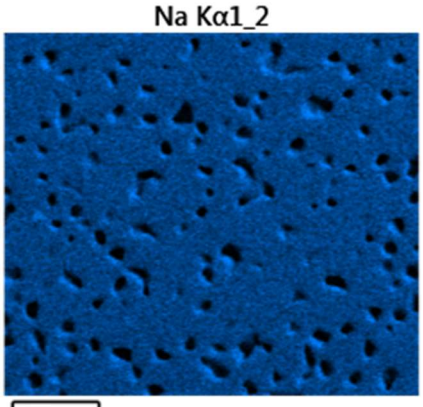
Na Kα1_2
25μm

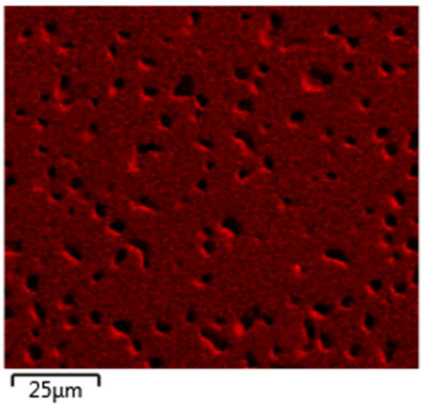
O Kα1
25μm

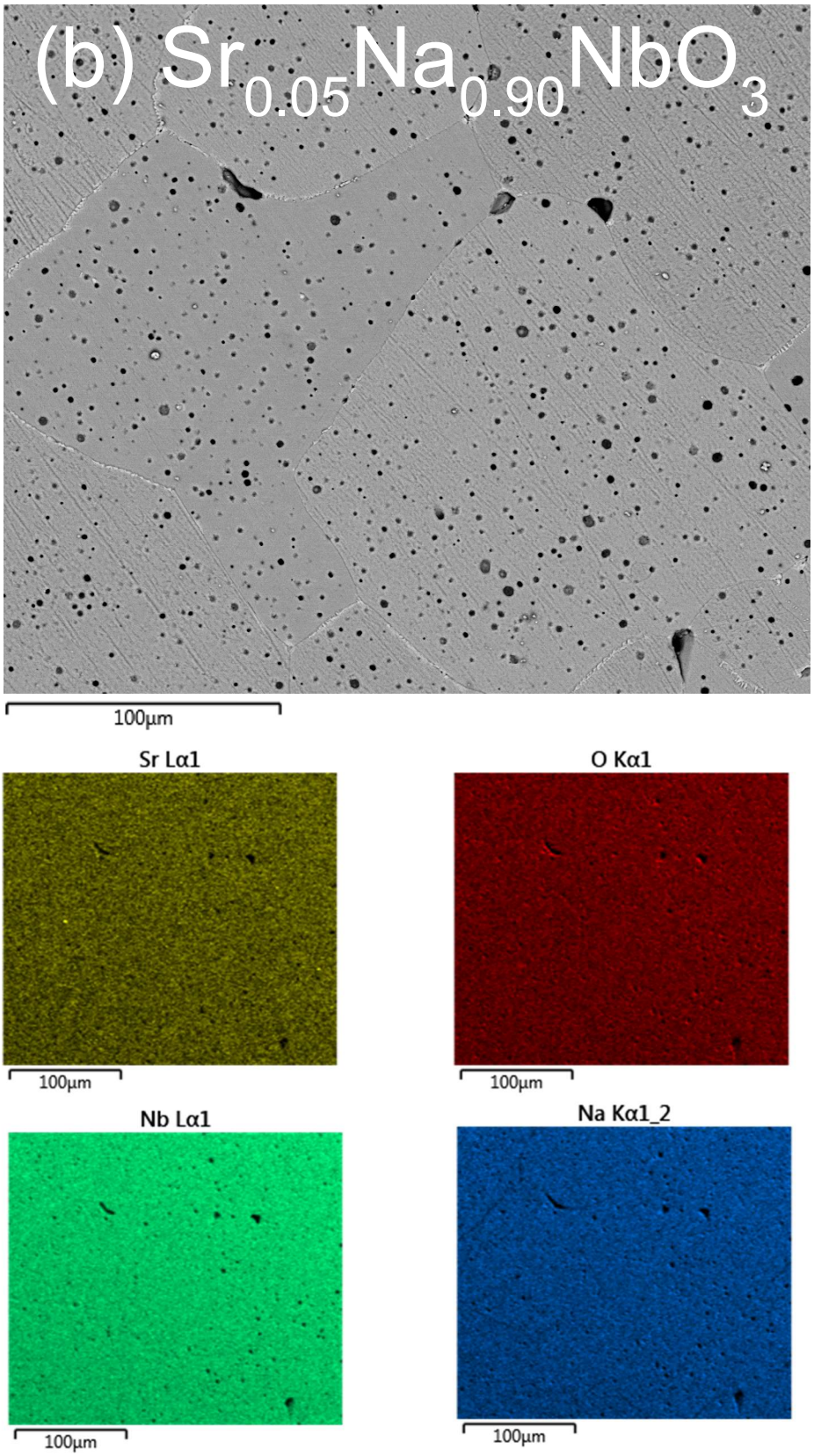
(b) $Sr_{0.05}Na_{0.90}NbO_3$
100μm
Sr Lα1
100μm
O Kα1
100μm
Nb Lα1
100μm
Na Kα1_2
100μm

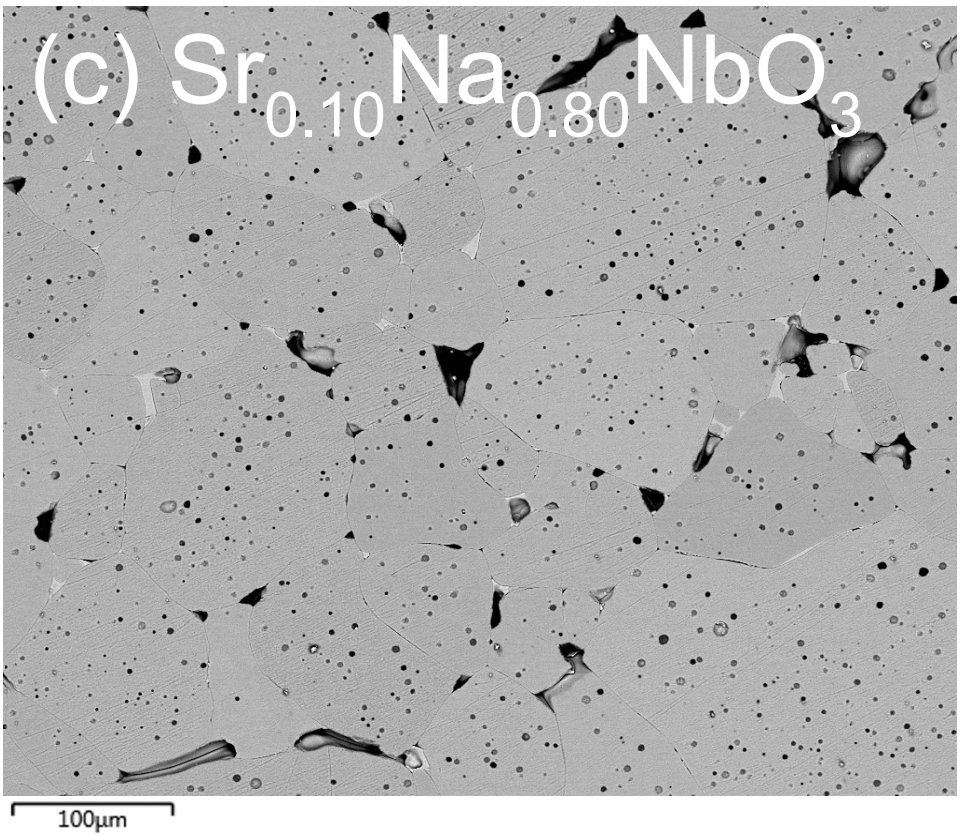
(c) $Sr_{0.10}Na_{0.80}NbO_3$
100µm

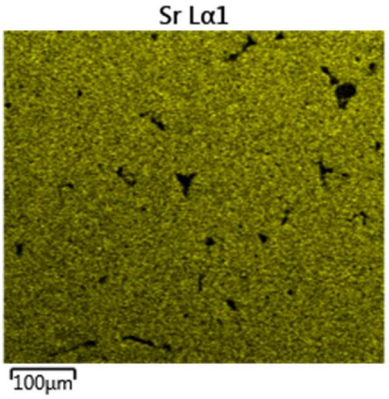
Sr Lα1
100µm

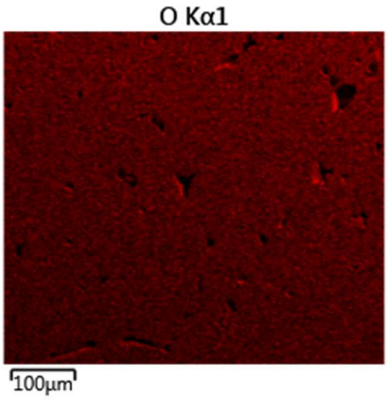
O Kα1
100µm

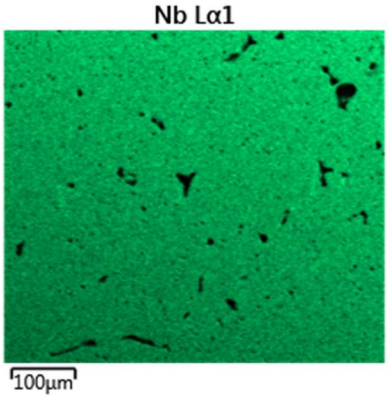
Nb Lα1
100µm

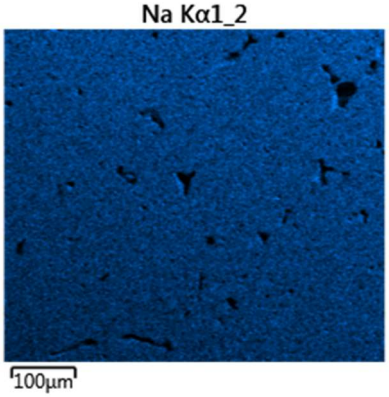
Na Kα1_2
100µm

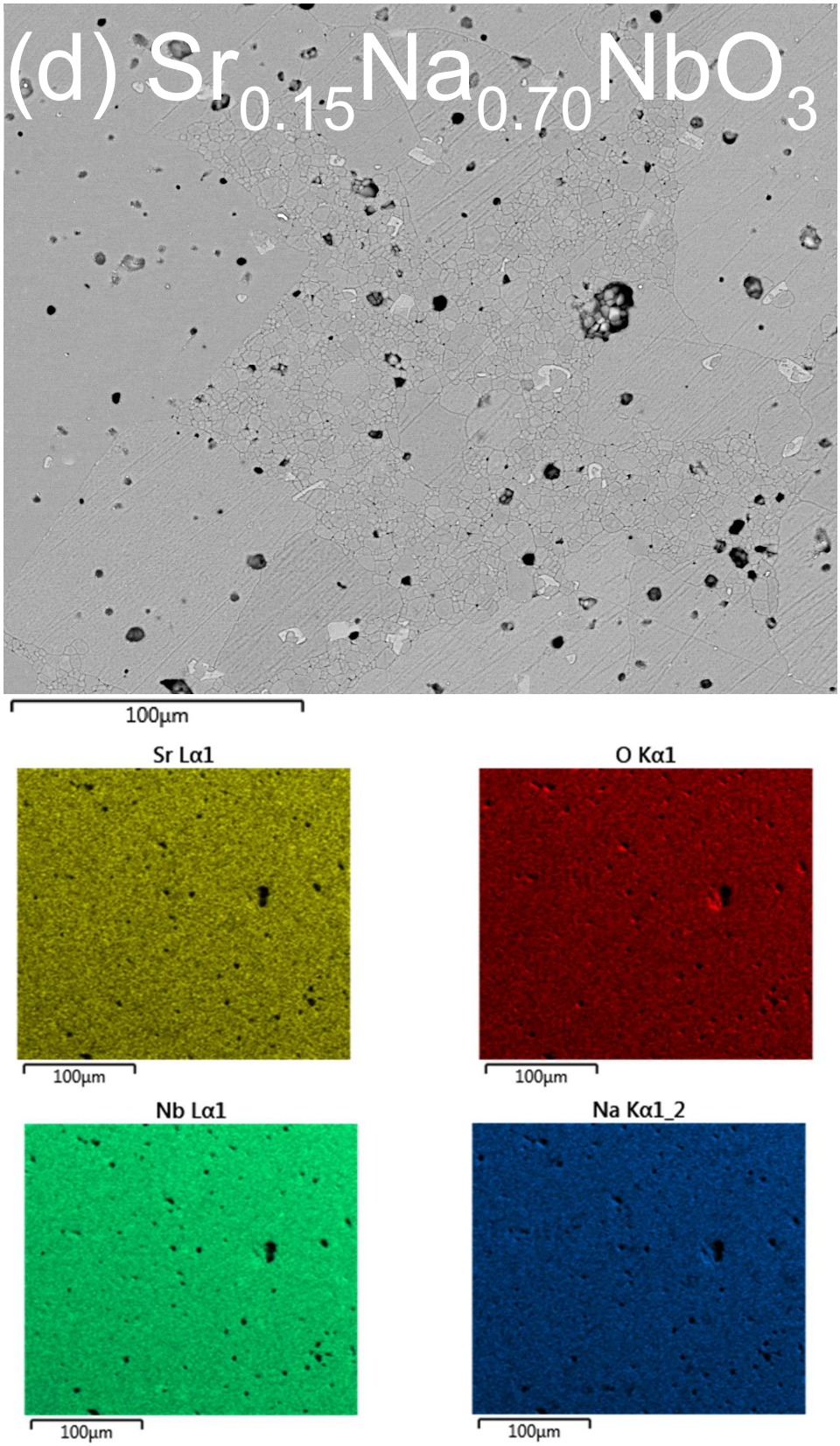
(d) $Sr_{0.15}Na_{0.70}NbO_3$
100μm
Sr Lα1
100μm
O Kα1
100μm
Nb Lα1
100μm
Na Kα1_2
100μm

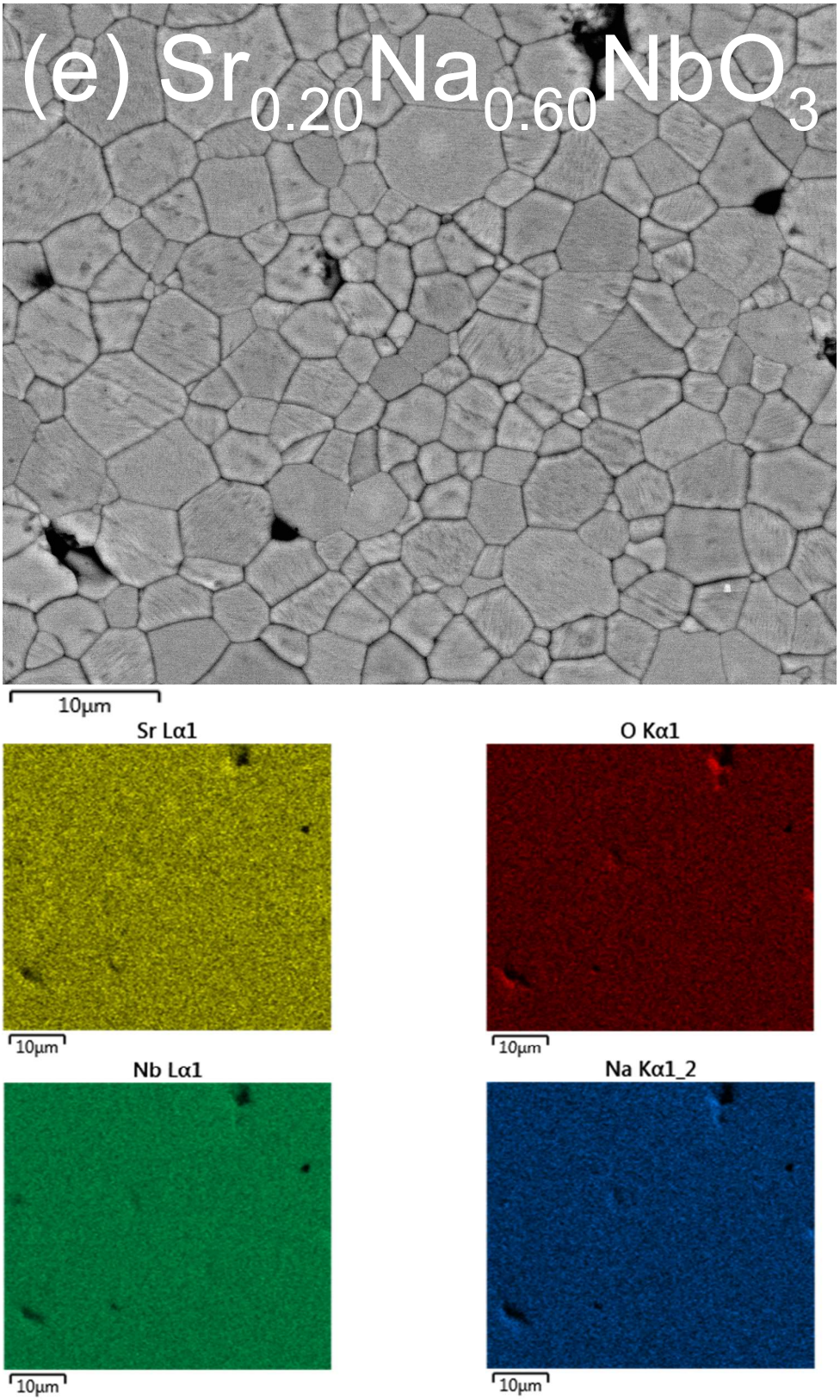
(e) $Sr_{0.20}Na_{0.60}NbO_3$
10μm
Sr Lα1
10μm
O Kα1
10μm
Nb Lα1
10μm
Na Kα1_2
10μm

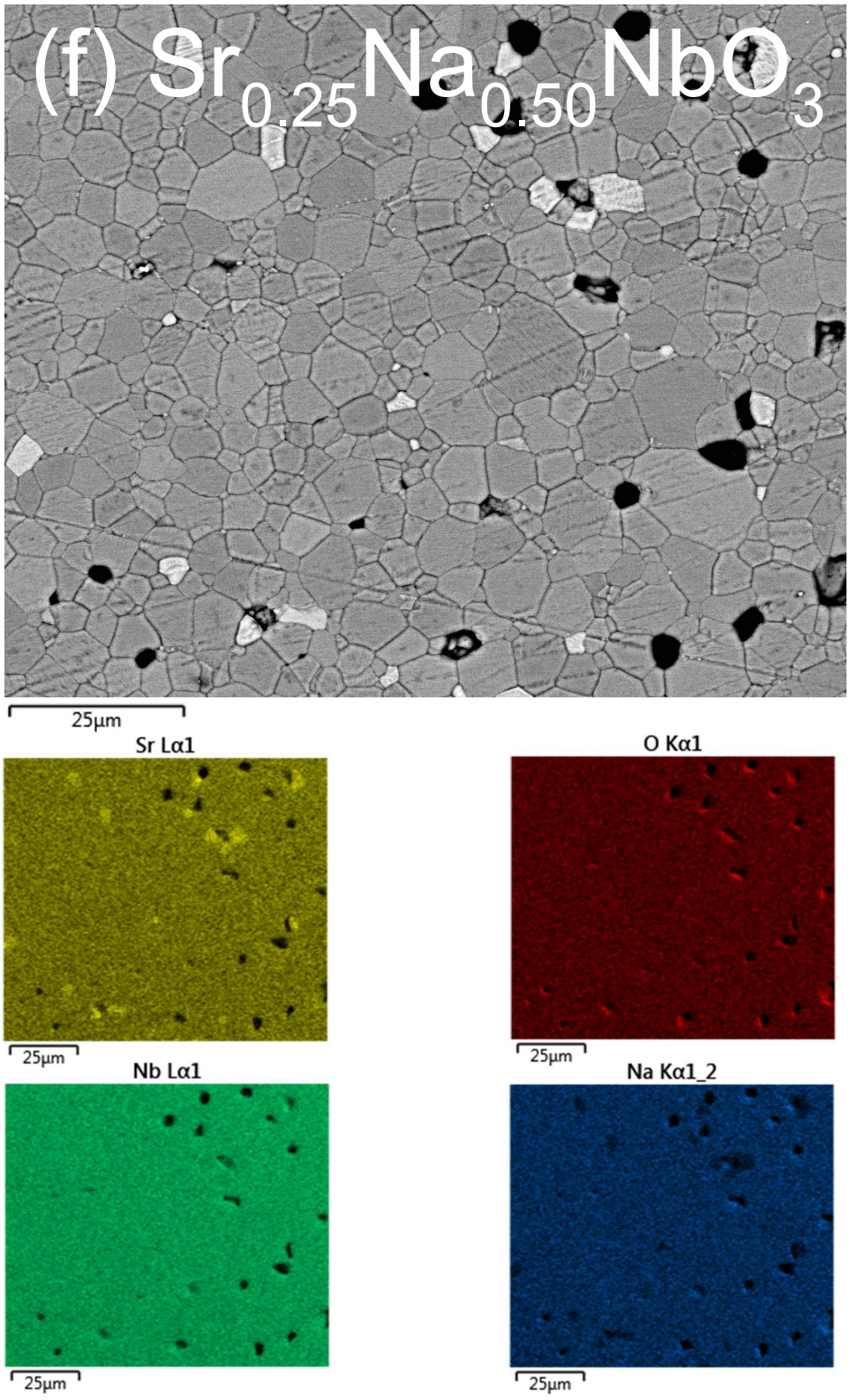

Figure S10: Backscatter electron micrographs and corresponding EDX maps of polished and thermally etched samples of (a) $NaNbO_3$, (b) $Sr_{0.05}Na_{0.90}NbO_3$, (c) $Sr_{0.10}Na_{0.80}NbO_3$, (d) $Sr_{0.15}Na_{0.70}NbO_3$, (e) $Sr_{0.20}Na_{0.60}NbO_3$, and (f) $Sr_{0.25}Na_{0.50}NbO_3$. Bright regions in (c) and (d) can be identified as $NaNb_3O_8$ and in (f) as tetragonal tungsten bronze $Sr_2NaNb_5O_{15}$

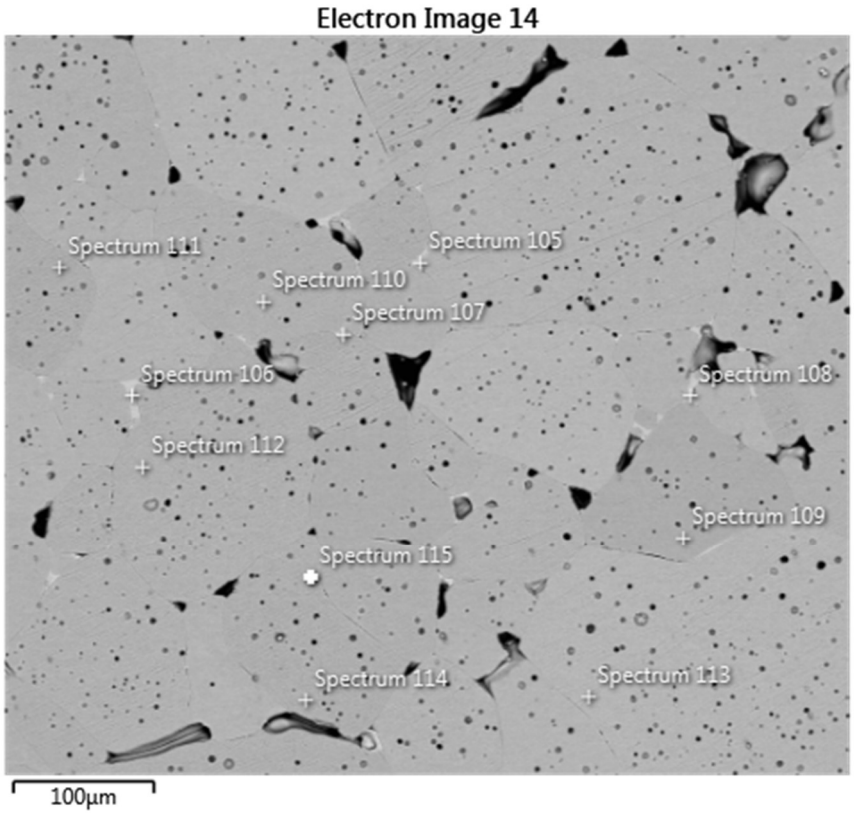

Figure S11: Backscattered electron micrograph of polished and thermally etched $Sr_{0.10}Na_{0.80}NbO_3$ bulk ceramic, annotated with point spectra positions.

Table S1: Spectrum number according to Figure S11, and corresponding atomic percentage of ions. Highlighted cells correspond to regions of bright contrast.

Spectrum	O (at%)	Na (at%)	Sr (at%)	Nb (at%)
105	63.22	8.74	0.3	27.73
106	61.53	9.08	0.47	28.93
107	62.8	9.87	0.5	26.82
108	62.43	9.01	0.18	28.39
109	57.29	16.14	2.18	24.4
110	57.53	16.59	2.1	23.78
111	58.05	15.83	2.11	24.02
112	57.17	16.67	2.13	24.03
113	57.7	16.23	2.15	23.92
114	58.74	16.23	2.06	22.96
115	57.52	15.8	2.1	24.58

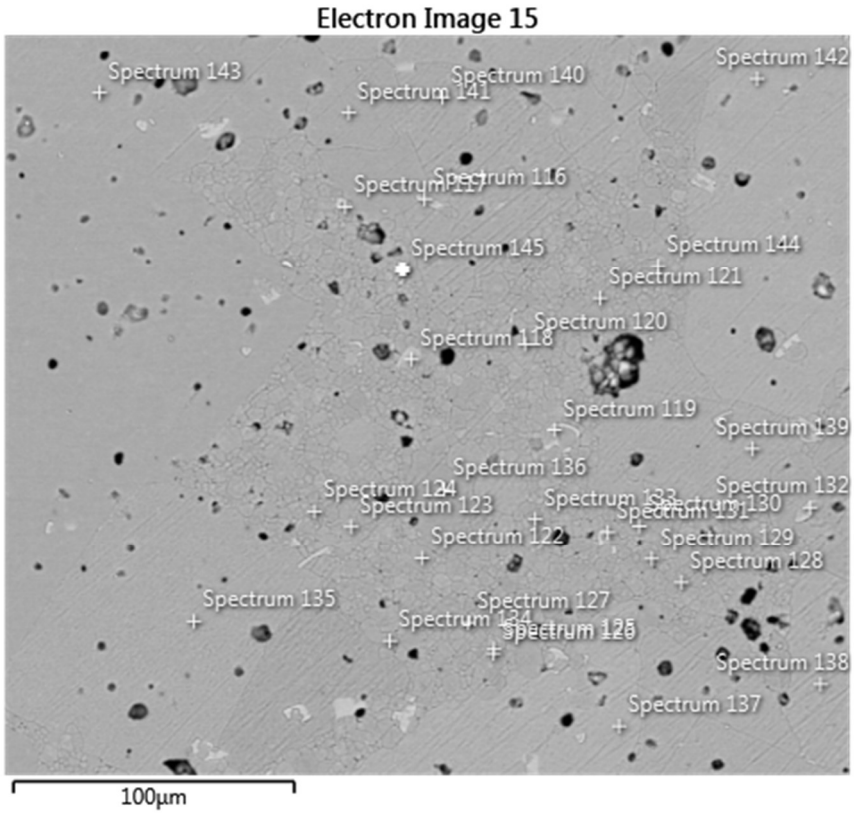

Figure S12: Backscattered electron micrograph of polished and thermally etched $Sr_{0.15}Na_{0.70}NbO_3$ bulk ceramic, annotated with point spectra positions.

Table S2: Spectrum number according to Figure S12, and corresponding atomic percentage of ions. Highlighted cells correspond to regions of bright contrast.

Spectrum	O	Na	Sr	Nb
116	63.49	7.29	1.89	27.33
117	63.3	7.59	1.8	27.32
118	62.33	7.51	1.83	28.34
119	63.21	7.46	1.79	27.55
120	58.67	14.3	3.25	23.79
121	58.56	14.28	3.18	23.98
122	58.56	14.25	3.24	24.01
123	57.84	14.53	3.07	24.56

124	57.29	14.53	3.41	24.78
125	59.72	14.55	2.91	22.82
126	58.28	14.07	3.38	24.27
127	57.96	14.33	3.21	24.51
128	58.14	14.85	3	24.01
129	58.17	14.1	3.29	24.44
130	58.36	14.3	3.19	24.15
131	64.44	8.15	1.83	25.58
132	61.88	7.43	1.97	28.72
133	59.27	13.94	3.19	23.59
134	58.47	13.93	3.32	24.28
135	58.88	13.63	3.47	24.03
136	58.27	14.13	3.28	24.32
137	59.66	14.01	3.14	23.19
138	57.49	14.33	3.21	24.97

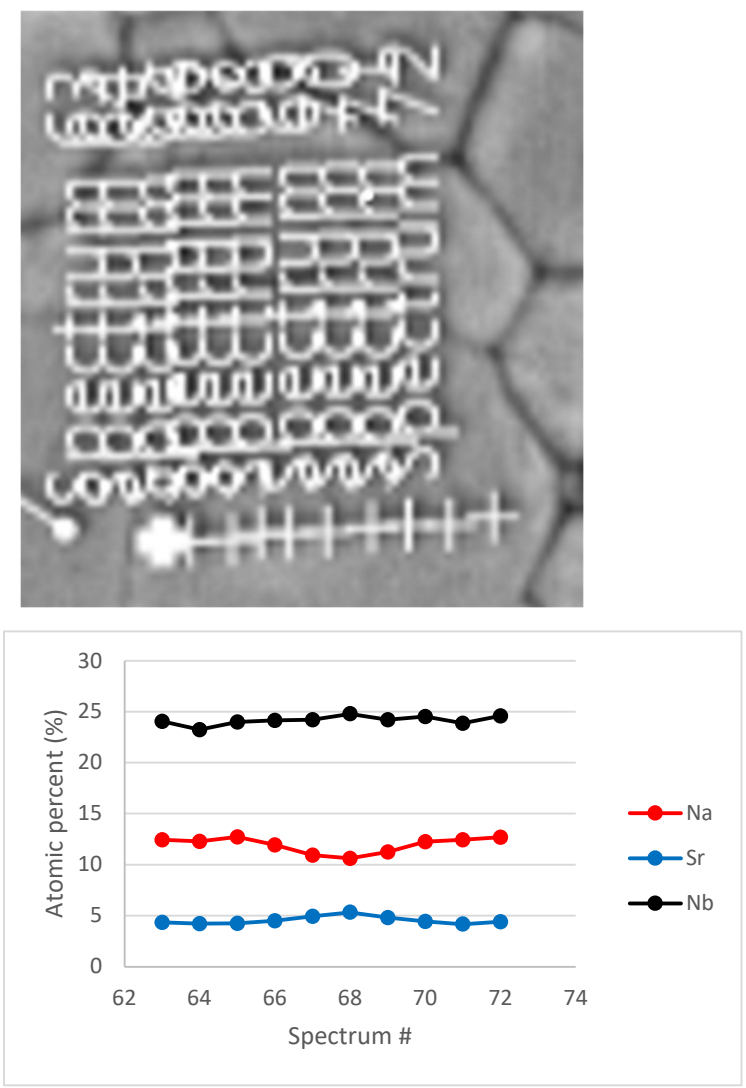

Figure S13: Point spectra across a grain in polished and thermally etched $Sr_{0.20}Na_{0.60}NbO_3$ and corresponding atomic percentage to demonstrate core-shell microstructure.

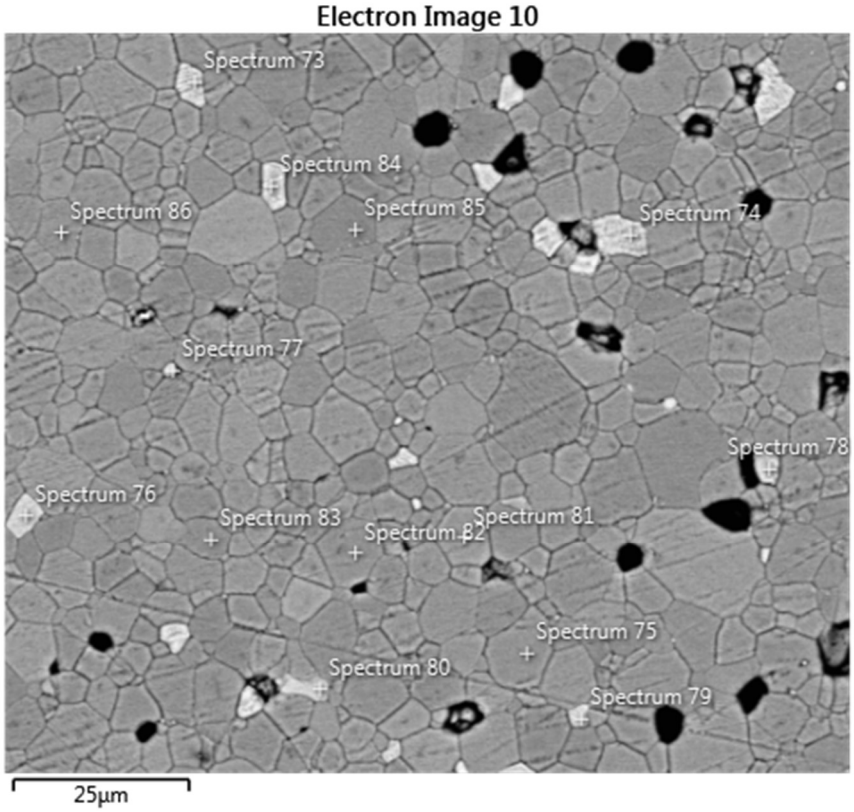

Figure S14: Backscattered electron micrograph of polished and thermally etched $Sr_{0.25}Na_{0.50}NbO_3$ bulk ceramic, annotated with point spectra positions.

Table S3: Spectrum number according to Figure S14, and corresponding atomic percentage of ions. Highlighted cells correspond to regions of bright contrast.

Spectrum	O (at%)	Na (at%)	Sr (at%)	Nb (at%)
73	61.25	4.95	8.09	25.71
74	63.05	4.28	8.36	24.32
75	58.45	10.41	5.67	25.48
76	60.43	4.13	9.02	26.42
77	44.97	9.85	7.68	37.5
78	59.76	4.55	8.88	26.82
79	61.37	5.25	8.03	25.35

80	60.47	5.34	7.96	26.23
81	59.34	10.31	5.58	24.77
82	58.85	10.56	5.64	24.95
83	58.84	10.35	5.59	25.22
84	60.53	4.29	9.14	26.05
85	58.28	10.69	5.7	25.33
86	59.3	10.38	5.63	24.69

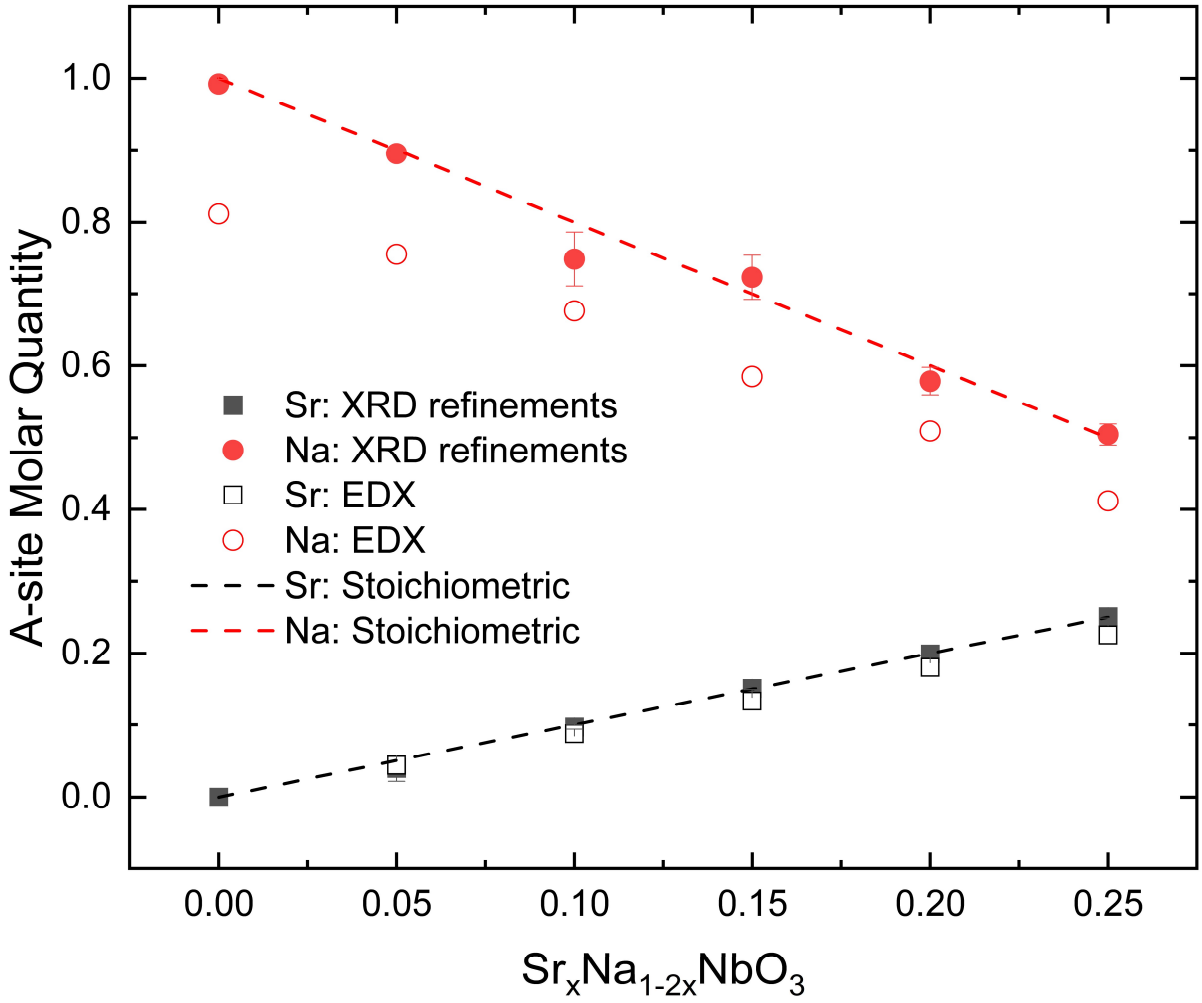

Figure S15: Sr^{2+} and Na^{+} occupancies extracted from Rietveld refinements (solid data points) and average at% calculated from EDX mapping (hollow data points) against composition. Dashed lines correspond to nominal $Sr_xNa_{1-2x}NbO_3$

SI Section S5: Dielectric Spectroscopy

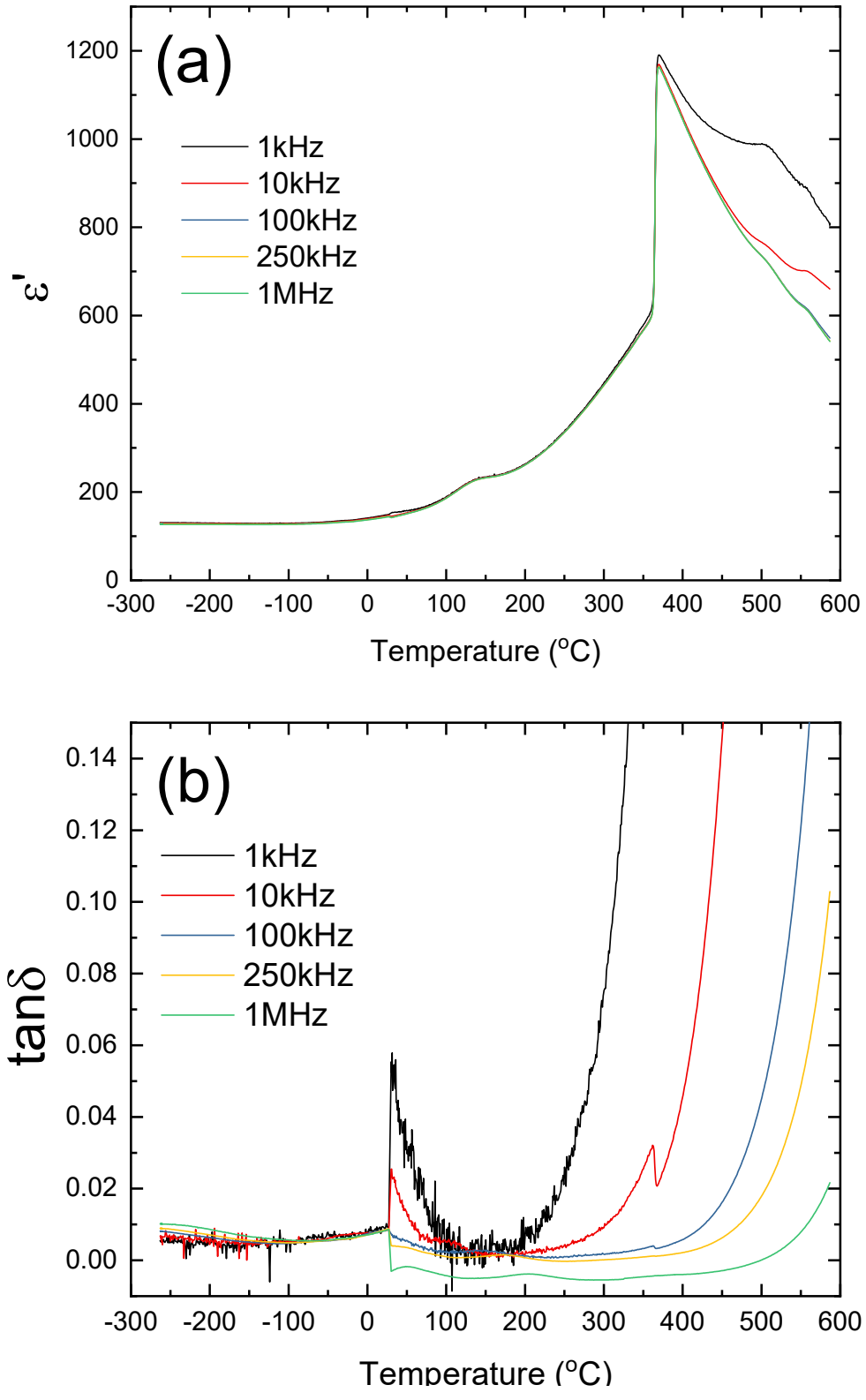

Figure S16: (a) Real component of permittivity (ε') and (b) tan δ at fixed frequencies against temperature for $NaNbO_3$ (x = 0.00). Sub-zero tan δ are due to electrical noise (inductance) from electrical testing equipment.

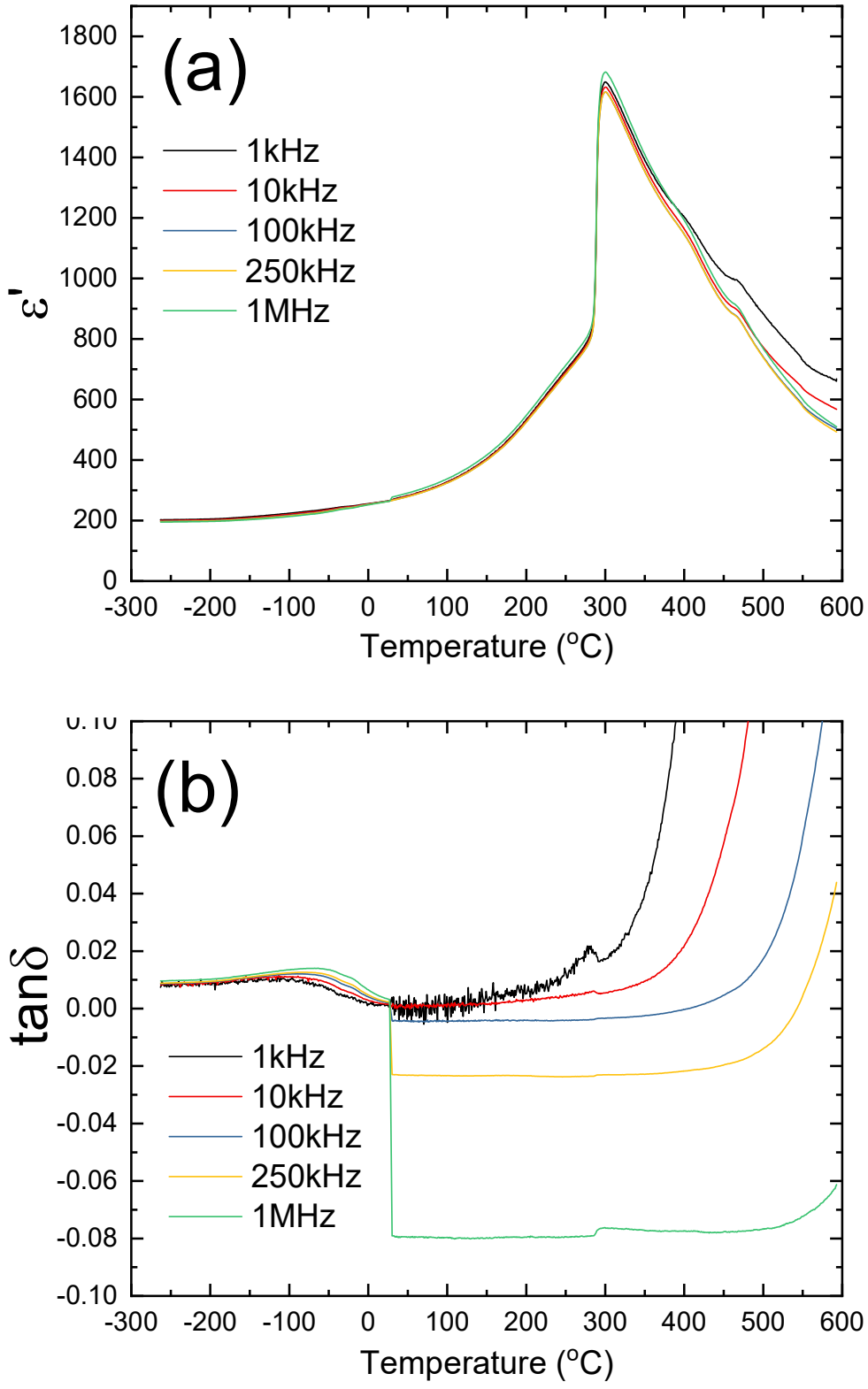

Figure S17: (a) Real component of permittivity (ε') and (b) tan δ at fixed frequencies against temperature for $Sr_{0.05}Na_{0.90}NbO_3$ (x = 0.05). Sub-zero tan δ are due to electrical noise (inductance) from electrical testing equipment.

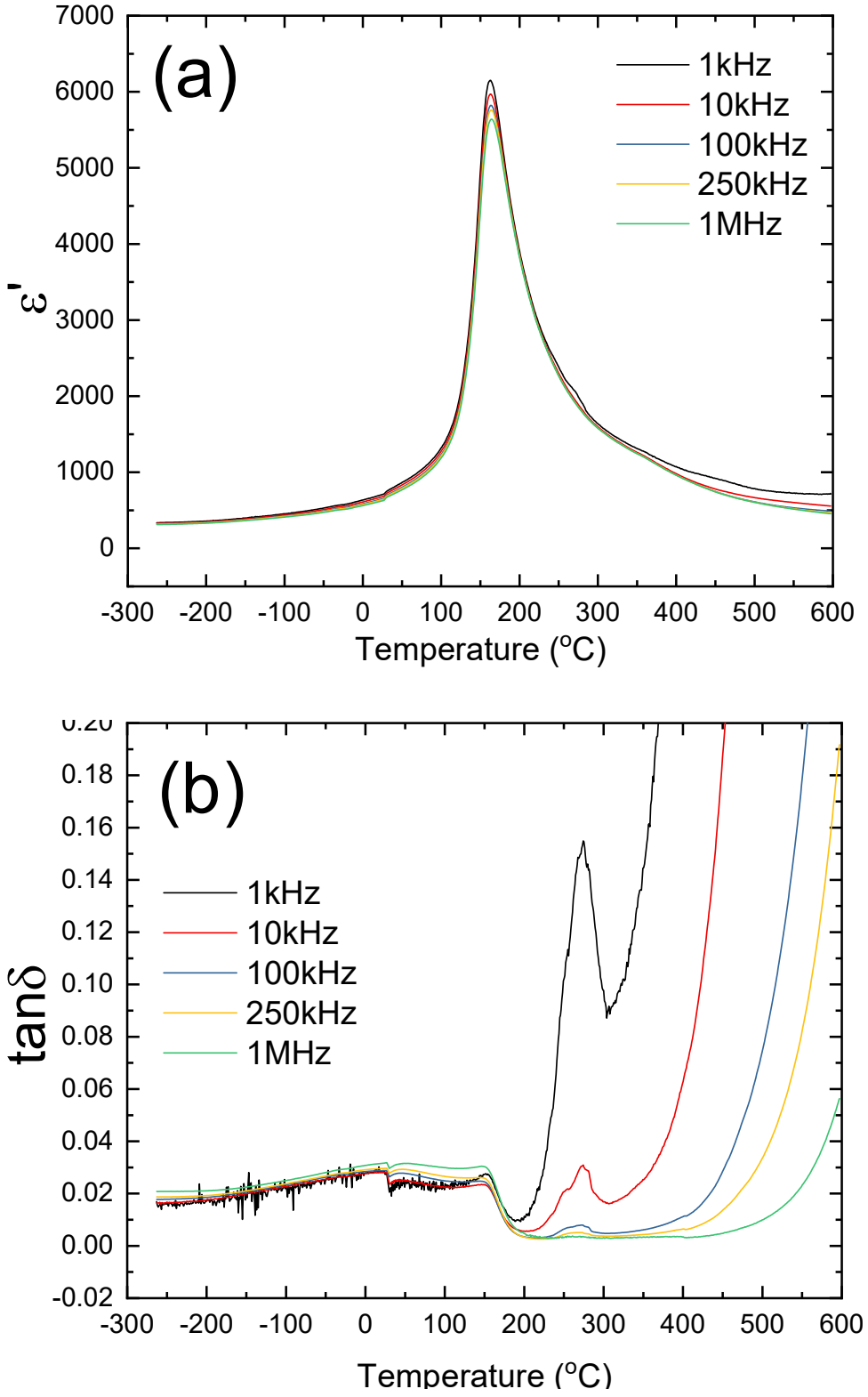

Figure S18: (a) Real component of permittivity (ε') and (b) tan δ at fixed frequencies against temperature for $Sr_{0.10}Na_{0.80}NbO_3$ (x = 0.10)

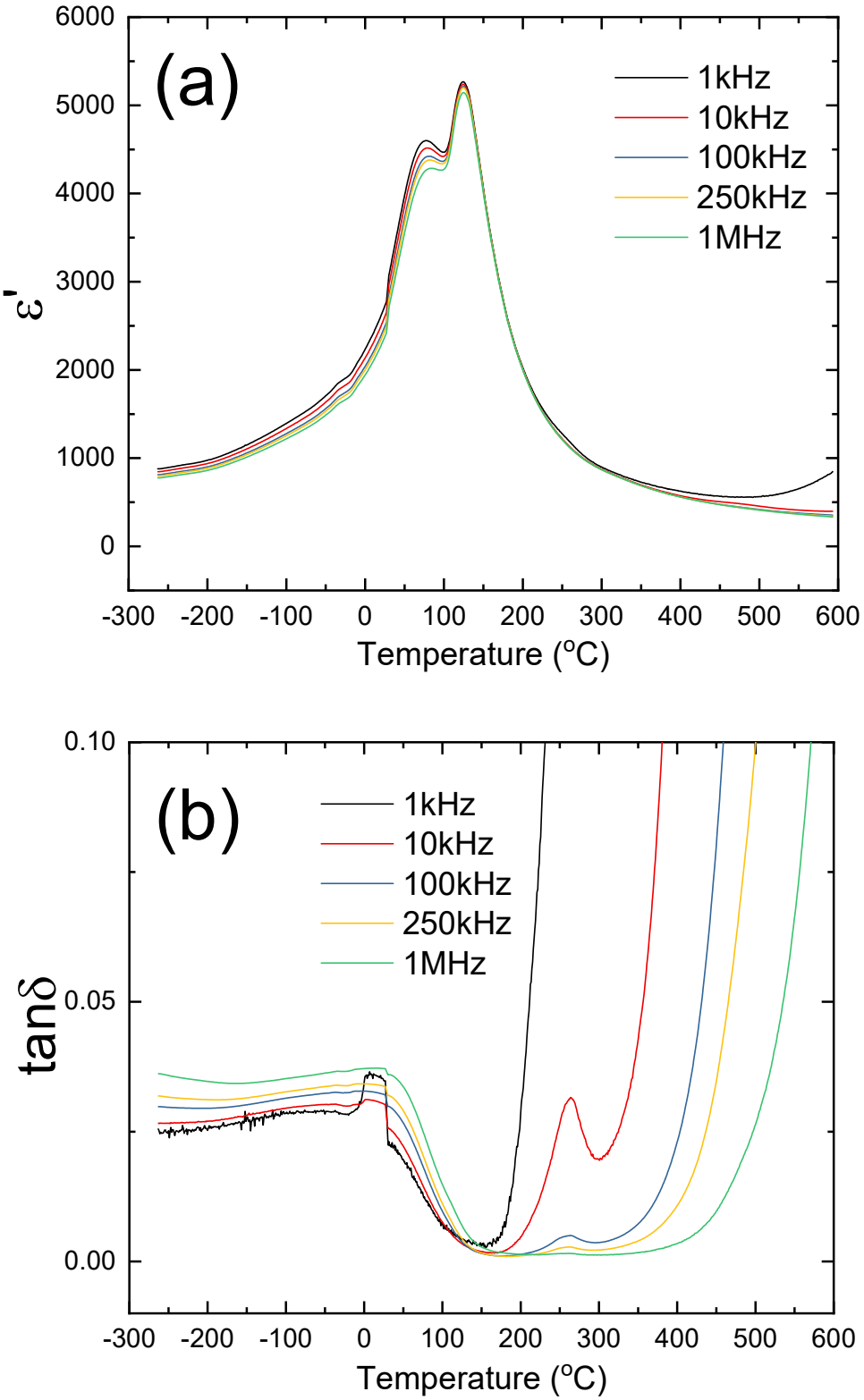

Figure S19: (a) Real component of permittivity (ε') and (b) tan δ at fixed frequencies against temperature for $Sr_{0.15}Na_{0.70}NbO_3$ (x = 0.15)

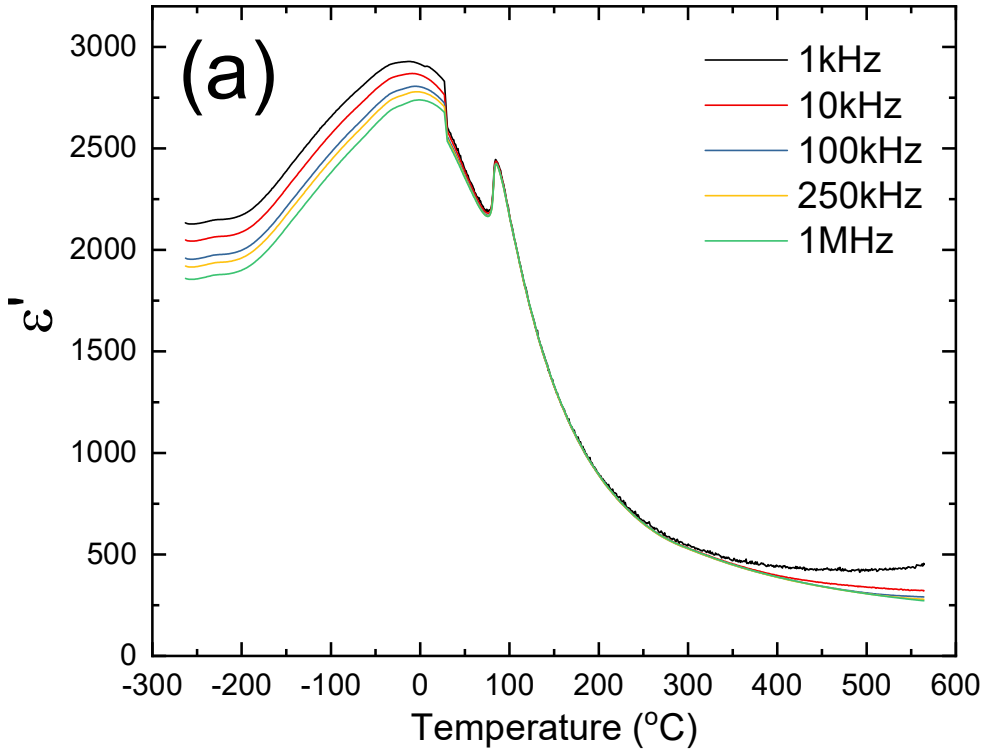

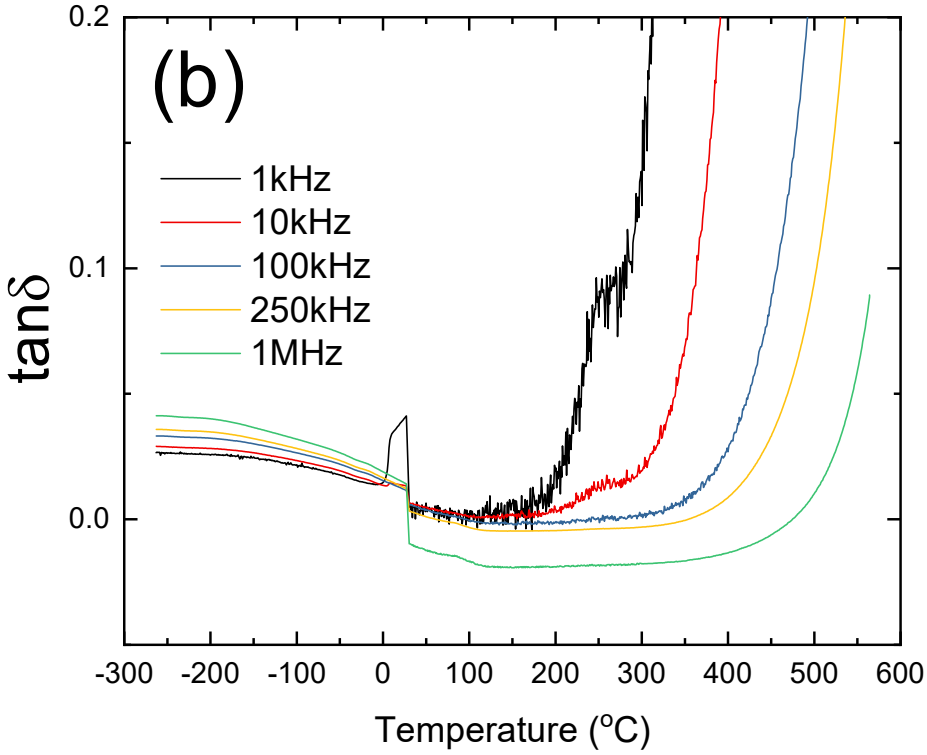

Figure S20: (a) Real component of permittivity (ε') and (b) tan δ at fixed frequencies against temperature for $Sr_{0.20}Na_{0.60}NbO_3$ (x = 0.20). Sub-zero tan δ are due to electrical noise (inductance) from electrical testing equipment.

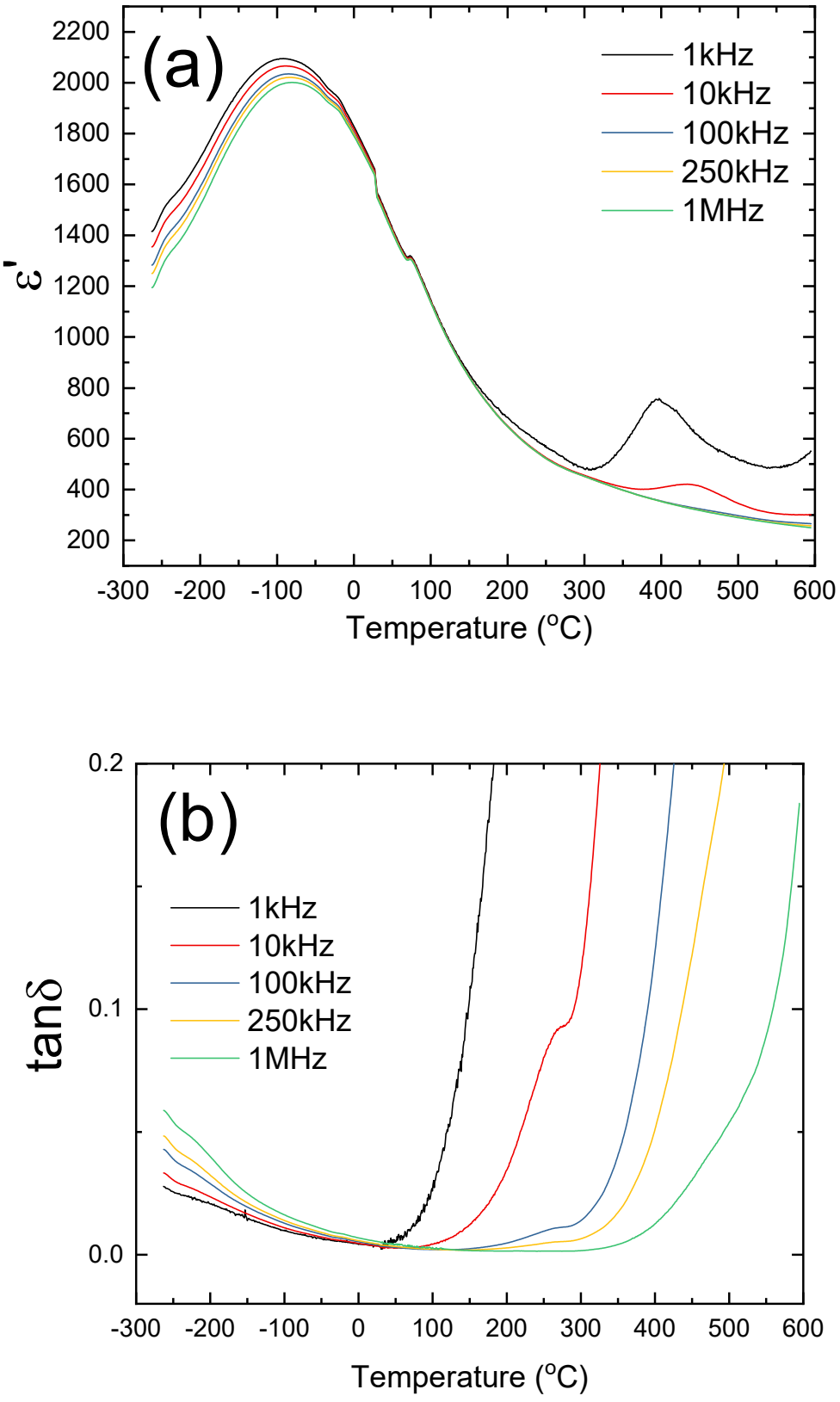

Figure S21: (a) Real component of permittivity (ε') and (b) tan δ at fixed frequencies against temperature for $Sr_{0.25}Na_{0.50}NbO_3$ (x = 0.25)

SI Section S6: Polarisation vs Electric Field analysis

Table S4: Maximum polarisation (P_{max}), remnant polarisation (P_R), coercive filed (E_C), recoverable energy density (W_{rec}), energy loss density (W_{loss}), thickness (S) over electrode radius (r), and efficiency ($W_{rec}/W_{rec}+W_{loss}$) for $Sr_xNa_{1-2x}NbO_3$ (x = 0.00, 0.05, 0.10, 0.15, 0.20, 0.25) at 40 $kV.cm^{-1}$

$Sr_xNa_{1-2x}NbO_3$	P_{max} ($\mu C.cm^{-2}$)	P_R ($\mu C.cm^{-2}$)	E_C ($kV.cm^{-1}$)	W_{rec} ($mJ.cm^{-3}$)	W_{loss} ($mJ.cm^{-3}$)	S/r	η (%)
0	1.03	0.31	9.94	12.4	16.5	0.34	42.9
0.05	1.49	0.37	9.90	20.5	22.3	0.36	47.8
0.1	6.63	4.60	17.58	25.3	120.3	0.37	17.4
0.15	14.19	6.43	8.01	100.5	162.9	0.35	38.2
0.20	9.63	0.30	1.60	173.4	20.9	0.45	89.2
0.25	6.57	2.04	11.85	71.4	96.7	0.42	42.5

SI Section S7: Impedance Spectroscopy and Arrhenius plots

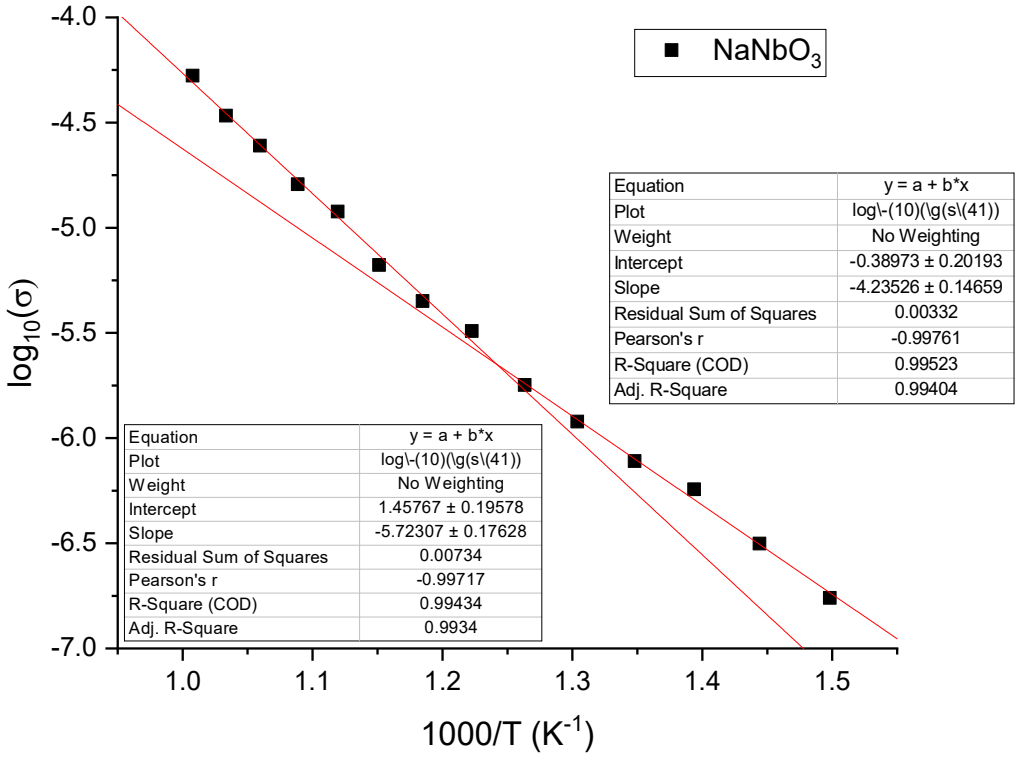

Equation	y = a + b*x
Plot	log\-(10)(\g(s\(41))
Weight	No Weighting
Intercept	-0.38973 ± 0.20193
Slope	-4.23526 ± 0.14659
Residual Sum of Squares	0.00332
Pearson's r	-0.99761
R-Square (COD)	0.99523
Adj. R-Square	0.99404

Equation	y = a + b*x
Plot	log\-(10)(\g(s\(41))
Weight	No Weighting
Intercept	1.45767 ± 0.19578
Slope	-5.72307 ± 0.17628
Residual Sum of Squares	0.00734
Pearson's r	-0.99717
R-Square (COD)	0.99434
Adj. R-Square	0.9934

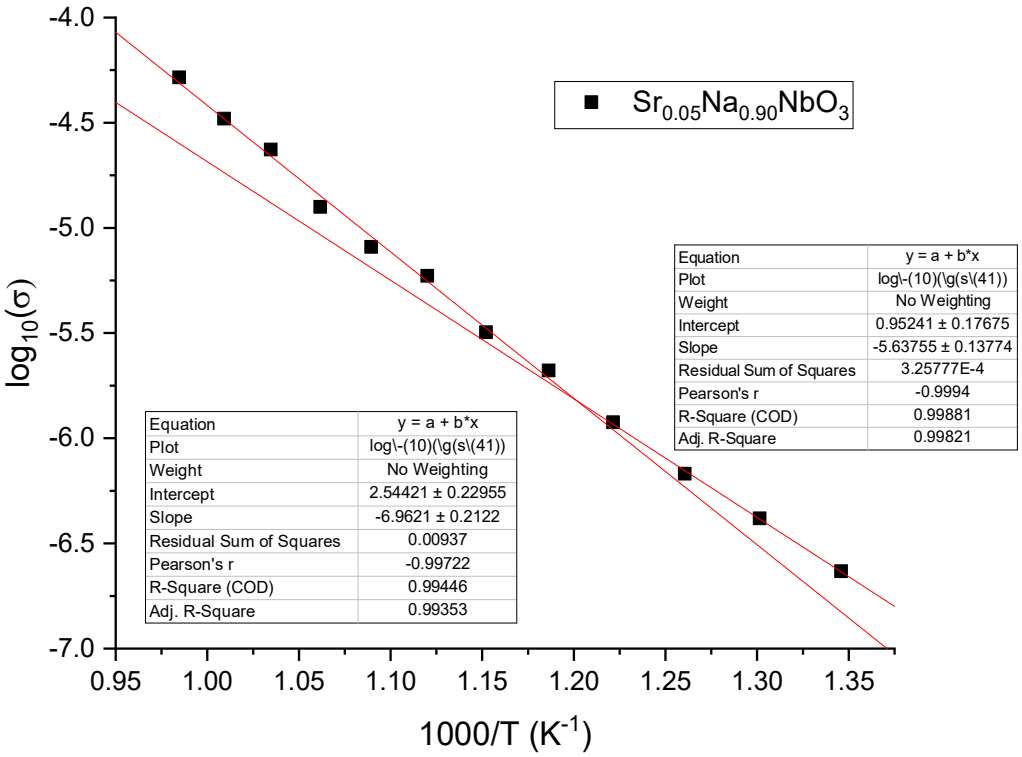

Equation	y = a + b*x
Plot	log\-(10)(\g(s\(41))
Weight	No Weighting
Intercept	0.95241 ± 0.17675
Slope	-5.63755 ± 0.13774
Residual Sum of Squares	3.25777E-4
Pearson's r	-0.9994
R-Square (COD)	0.99881
Adj. R-Square	0.99821

Equation	y = a + b*x
Plot	log\-(10)(\g(s\(41))
Weight	No Weighting
Intercept	2.54421 ± 0.22955
Slope	-6.9621 ± 0.2122
Residual Sum of Squares	0.00937
Pearson's r	-0.99722
R-Square (COD)	0.99446
Adj. R-Square	0.99353

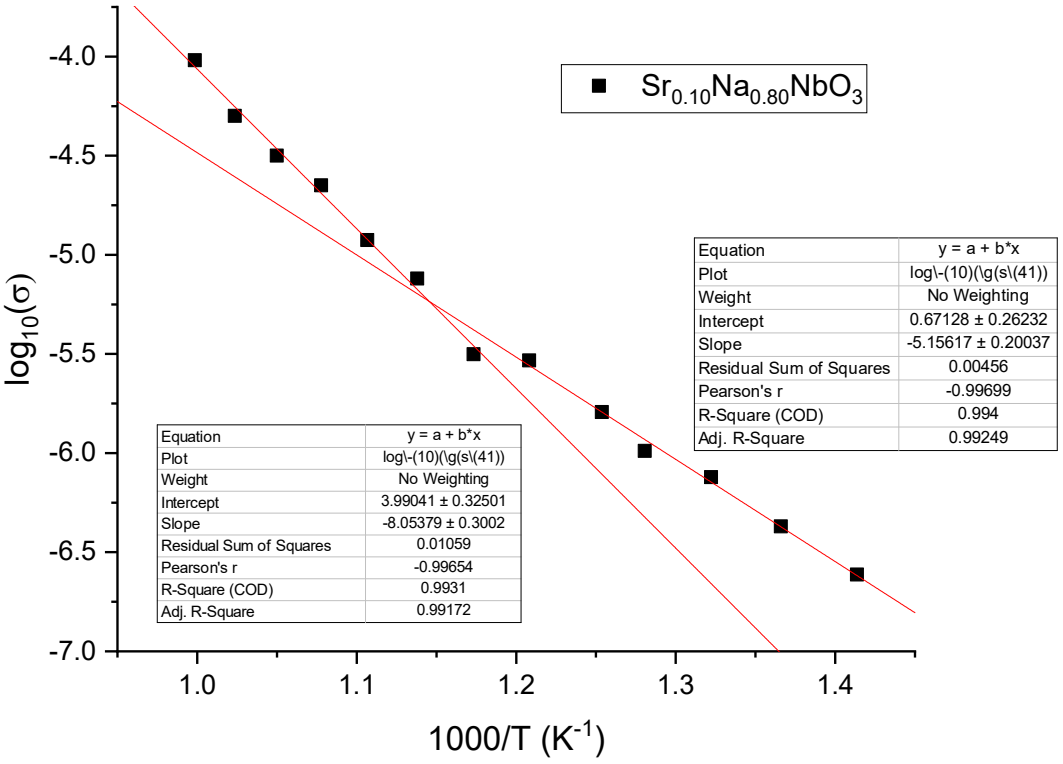

Equation	y = a + b*x
Plot	log\-(10)(\g(s\(41))
Weight	No Weighting
Intercept	3.99041 ± 0.32501
Slope	-8.05379 ± 0.3002
Residual Sum of Squares	0.01059
Pearson's r	-0.99654
R-Square (COD)	0.9931
Adj. R-Square	0.99172

Equation	y = a + b*x
Plot	log\-(10)(\g(s\(41))
Weight	No Weighting
Intercept	0.67128 ± 0.26232
Slope	-5.15617 ± 0.20037
Residual Sum of Squares	0.00456
Pearson's r	-0.99699
R-Square (COD)	0.994
Adj. R-Square	0.99249

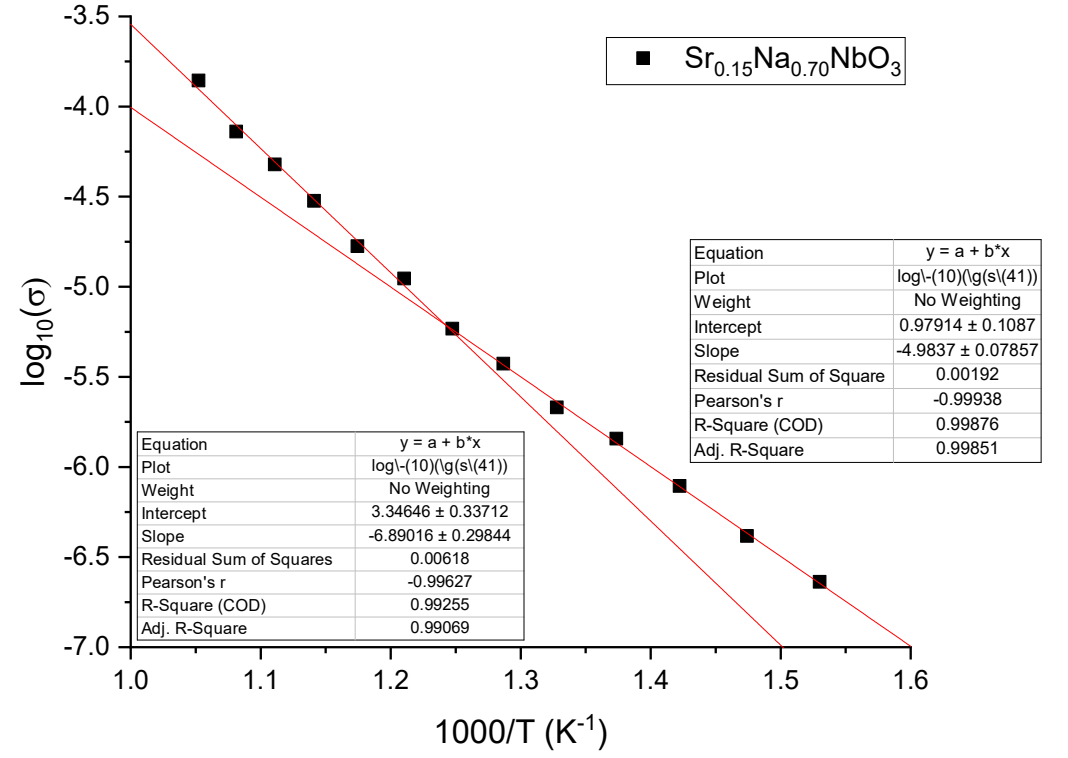

Equation	y = a + b*x
Plot	log\-(10)(\g(s\(41))
Weight	No Weighting
Intercept	3.34646 ± 0.33712
Slope	-6.89016 ± 0.29844
Residual Sum of Squares	0.00618
Pearson's r	-0.99627
R-Square (COD)	0.99255
Adj. R-Square	0.99069

Equation	y = a + b*x
Plot	log\-(10)(\g(s\(41))
Weight	No Weighting
Intercept	0.97914 ± 0.1087
Slope	-4.9837 ± 0.07857
Residual Sum of Square	0.00192
Pearson's r	-0.99938
R-Square (COD)	0.99876
Adj. R-Square	0.99851

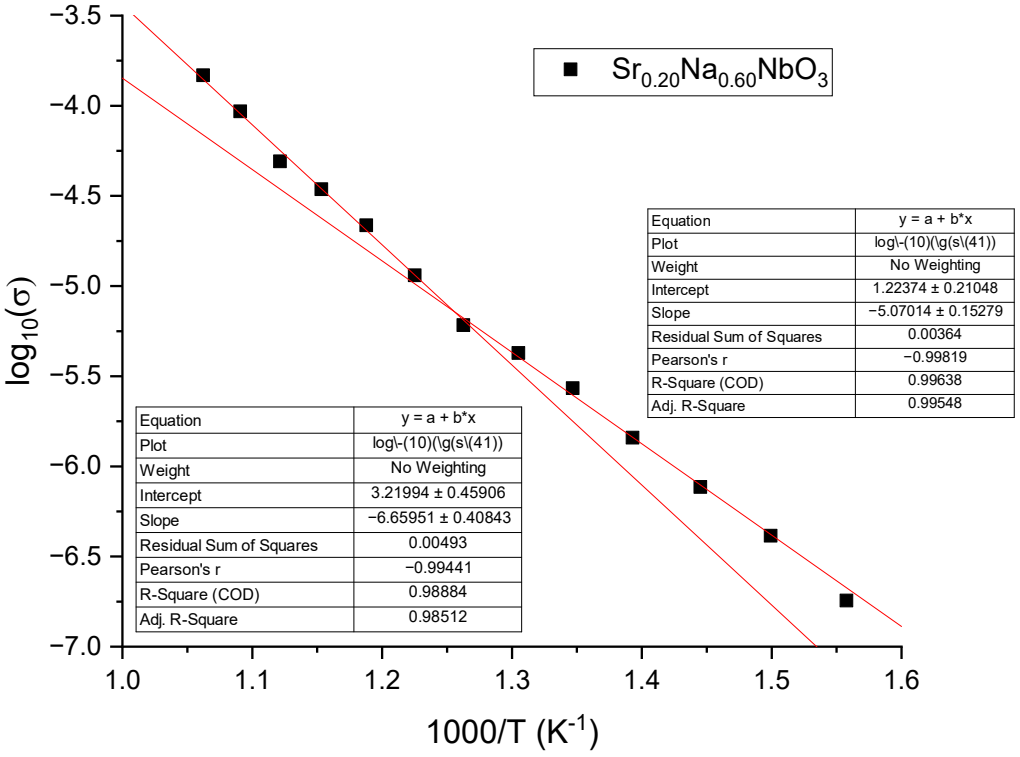

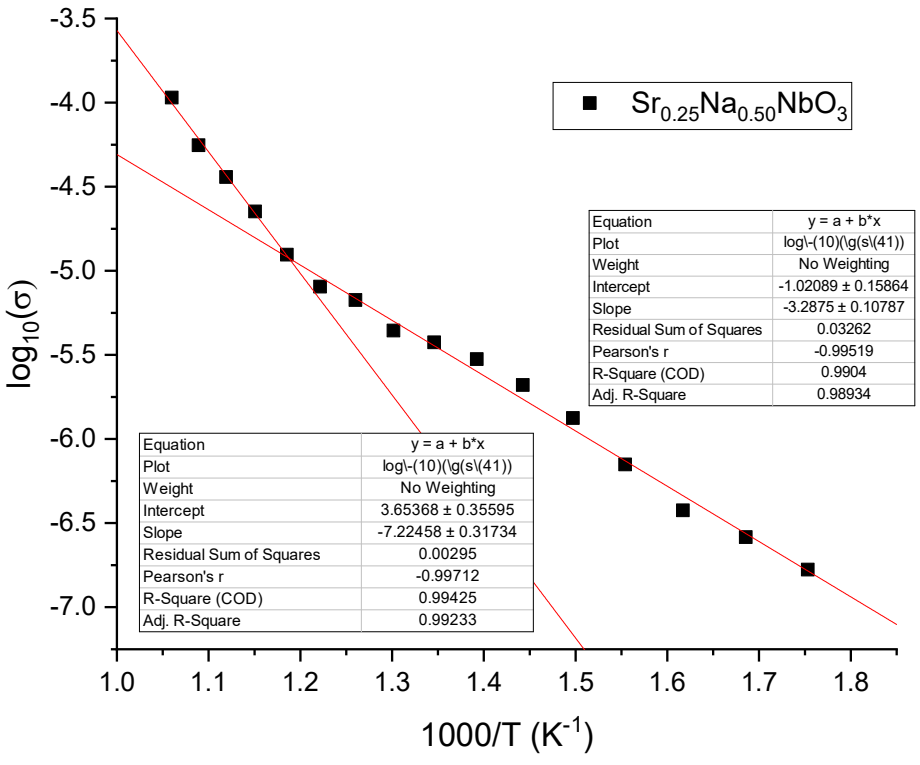

Figure S22: Arrhenius plots of conductivity calculated using M'' at the relaxation frequency for (a) $NaNbO_3$, (b) $Sr_{0.05}Na_{0.90}NbO_3$, (c) $Sr_{0.10}Na_{0.80}NbO_3$, (d) $Sr_{0.15}Na_{0.70}NbO_3$, (e) $Sr_{0.20}Na_{0.60}NbO_3$, and (f) $Sr_{0.25}Na_{0.50}NbO_3$.

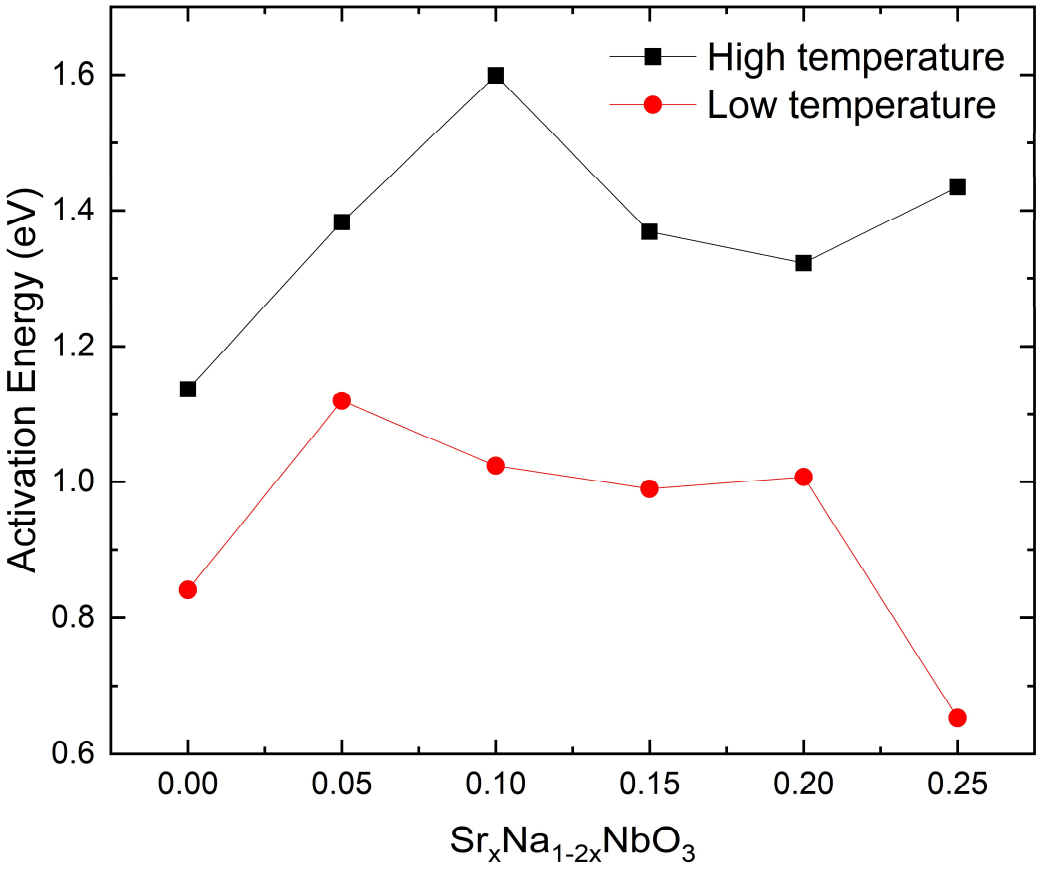

Figure S23: High temperature and low temperature activation energies extrapolated from Arrhenius plots of conductivity against composition.